On the Rate of Refreezing in a Bore Hole in an Ice Shelf

Ken Hughes

UNIVERSITY *of* OTAGO

Te Whare Wānanga o Otāgo

NEW ZEALAND

A dissertation submitted for partial
fulfilment of the degree of

Bachelor of Science (Honours)

at the University of Otago,
Dunedin, New Zealand

September 2011

Abstract

Hot water drilling is a technique commonly used in the study of glaciers, ice shelves and the oceans or earth beneath them. Creating a bore hole allows access to regions under ice too thick to be drilled by other methods. The remoteness of the locations involved places limits on the availibility of resources and hence refreezing of these holes places a large restriction on the period of time they can be used. Prediction of the latter is the specifc challenge which this thesis addresses by creating a realistic model of the rate of refreezing. At the simplest level the bore hole needs to have a diameter larger than the instruments that have passed through it to allow for safe retrieval.

Two mathematical models based on the conservation of either salt or heat are created to simulate the closure of a bore hole drilled in the Ross Ice Shelf, Antarctica. The heat flux model uses a numerical solution to the heat conduction to model the evolution of the temperature distribution in the host ice. Ice growth is consequently calculated from the balance of this sensible heat and the latent heat released at the growing ice/water interface. The salinity variation model uses experimental data to find radius change from the salt budget in the bore hole assuming a closed system. Data for this thesis were provided by a field study undertaken by the National Institute of Water and Atmospheric Research (NIWA) in December 2010. The heat flux model broadly confirms predictions of the refreezing rates derived by the conservation of salt which is based on observation. This gives confidence in the generalisation of the heat flux model for predicting the rates of closure of other bore holes.

The predictions from both are subject to a large uncertainty due to the poorly defined value of the solid fraction of ice that refreezes, per unit volume of seawater, on the side of the bore hole. This is taken to be 0.4 throughout this study. The predicted rates are also strongly dependent on the initial conditions and the boundary conditions chosen but typical results show the diameter decreases by about $5 - 10$ mm hr^{-1}.

Acknowlededgments

Contents

Chapter 1

Introduction

1.1 Overview

The creation of a bore hole by hot water drilling enables scientific investigation of the regions within and underneath an ice shelf, ice sheet or glacier. These long, cylindrical, water-filled holes can be created rapidly but they promptly begin refreezing after drilling. Often the hole needs to be maintained with sufficient diameter for an extended period of time to undertake oceanographic measurements below an ice shelf. In order to safely retrieve any instruments that have been deployed, the hole cannot be left to refreeze so much that its diameter becomes less than the size of the devices being lowered through the hole. However, the closure of the hole is not easily logged and so to avoid the risk of any equipment getting trapped in the ice it must be removed well before the critical diameter is approached. Creating a model of ice growth in the bore hole will allow for more efficient use of time, money and resources when drilling in these remote environments.

This study aims to model the refreezing of a particular bore hole drilled in the Ross Ice Shelf (RIS). The hole was created for a study of the ocean beneath the ice shelf, undertaken by the National Institute of Water and Atmospheric Research (NIWA) starting in November 2010. Two approaches will be taken to model the change in radius upon closure. The first, described in Chapter 4, uses the principle of conservation of the mass of salt with down-hole measurements as inputs to the model. The second, described in Chapter 5, applies thermodynamic principles allowing the possiblity that the model be generalised to different bore holes. The compatibility of the predictions from these models is discussed in Chapter 6.

1.2 Measurements and Recordings

The purpose of the NIWA study was to obtain oceanographic information for the ANtarctic geological DRILLing (ANDRILL) project. This paleoclimatalogical project aims to reveal past glacial history and predict Earth's future climate by drilling deep into Antarctic sediment (more information can be found at www.andrill.org). Knowledge of the water column is needed to aid the design of a drill rig to be used to obtain sediment cores (personal communication, M. Williams). The study concerned four different bore hole sites, with an intensive oceanographic study undertaken at Hole 3, the hole that will be described in this study. The location of the bore hole site is shown in Figure 1.1 with more detail given in Chapter 2.

The data to be used in this study were taken over two 28 hour periods. During each period a Conductivity-Temperature-Depth (CTD) profiler (described in Section 2.3.1) was deployed 10 times from the ice shelf surface to measure temperature and salinity in
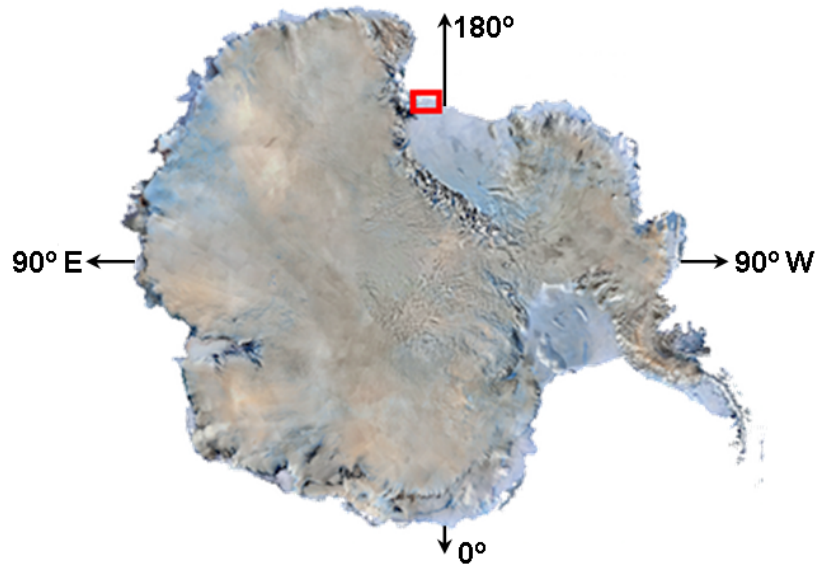
Figure 1.1: Map of Antartica identifying the location of the bore hole site. Image taken from www.andrill.org.

the sub-ice shelf ocean. In each of the 10 casts the profiler descended through the bore hole once, but was raised and lowered through the water underneath the ice shelf three times. The casts were regularly spaced with each taking approximately 150 minutes. The first and second 28 hour periods were approximately five days apart to allow measurement of the ocean properties during spring tide and neap tide, respectively.

The profiler used in this study had a maximum width of 225 mm. This provides a critical diameter that the bore hole cannot fall below.

Chapter 2

Background

2.1 Ice Shelves and Glaciers

Ice shelves are large, land-fastened ice sheets floating on the ocean. They are typically of the order of hundreds of metres in height, and akin to an iceberg, roughly one-ninth of that height is above water. As with any glacier ice shelves form as moving ice from the Antarctic continent is forced downward under gravity. They are a significant feature in Antarctica, surrounding approximately 44% of the coastline (Drewry, 1983). An ice shelf is not to be confused with sea ice which forms from the ocean freezing, has a thickness of the order of metres and contains a significant amount of salt in its bulk structure. An ice shelf contains ice formed due to the compaction of snow on land and consequently contains no salt.

The ice that glaciers consist of can be broadly classified into two categories, cold ice and temperate ice. Temperate ice is defined as ice with a temperature at the pressure melting point. Cold ice is defined as ice with a temperature below this (Greve and Blatter, 2009). Most ice in ice shelves, and ice sheets in general, falls into the category of cold ice.

2.1.1 The Ross Ice Shelf

The Ross Ice Shelf (RIS) is the world's largest, covering an area of 4.72×10^5 km^2 (Rafferty, 2011). Its thickness varies from approximately 700 m near the grounding line to 250 m at the ice front and it moves on the order of a few hundred metres per year (Paterson, 1969). At the NIWA bore hole site the ice shelf was floating upon 650 m of water.

2.1.2 Vertical Temperature Profile

The vertical temperature distribution of an ice shelf is of great importance when calculating the closure rate of a bore hole. The temperature has two boundary conditions, the surface and the base. The condition at the base is simplest and requires the temperature to be approximately equal to the freezing point of water at the base of the ice shelf. The freezing point is dependent on both salinity and pressure and would have been $-2.1°$C at the base of the bore hole in this study. The temperature in the top of the ice shelf changes with season; near the calving front of the RIS the temperature 2 m below the surface was measured to range between $-16°$C and $-31°$C during 2008 (MacAyeal et al., 2008). However, this effect is attenuated rapidly with depth and below 20 m the seasonal effect is negligible (Paterson, 1969). Excluding the upper 20 m of the ice shelf allows it to be considered in a steady state with respect to temperature.

The temperature of the ice around the NIWA hole was not measured at the same time as the water properties. Instead we use a profile from another site on the RIS that was 227 km away.

A full vertical temperature profile in the RIS was recorded in December 1958 at the Little America V station (LAV) with the results given in Bender and Gow (1961)[1].

NIWA Bore Hole Site	77°31'S 171°20'E
LAV	78°11'S 162°10'E

A temperature profile from LAV can confidently be used as an appropriate way to resolve the lack of temperature data at the NIWA bore hole location for several reasons:

- both sites are located near the ocean on the RIS with LAV only 70 km further south.

- the temperatures were recorded in December, the same month the present field study took place.

- the thicknesses of the RIS at the bore hole site was 252 m. The thickness at LAV was estimated to be $256 - 259$ m (so a vertical scaling of only a $2 - 3\%$ is required).

Humbert et al. (2005) give a discussion of their use of the data from LAV to determine a model temperature profile across the entire RIS. They initially attempted a least squares parabolic fit. However, a problem arises as this fit implies a slight temperature inversion in the top section of the ice shelf. They account for this by setting the coefficient of T^2 of the fit to the particular value which yields a vertical tangent to the temperature profile at the ice surface. Naturally some loss of accuracy accompanies this manipulation.

The top 38.5 m of the temperature profile are not of concern for this study (see Section 3.2) which means that a different approach to that of Humbert et al. (2005), that gives a more accurate fit, can be incorporated. A cubic spline (performed using the built in MatLab function 'spline') is applied to the data of Bender and Gow (1961) to interpolate between measurements and the result is scaled to fit the slightly smaller depth. The resultant model profile is given in Figure 2.1a.

2.1.3 Vertical Density Profile

An ice shelf is not composed completely of solid ice. A layer of compacted snow sits above a layer of low density ice, known as firn, that extends to approximately 50 m below the surface. The density is significantly lower at the top and increases monotonically with depth.

The density value with depth was also recorded by Bender and Gow (1961) at LAV and is shown in Figure 2.1b (also vertically scaled). Its change with depth is of less importance than that of the temperature, but nonetheless will be important in modelling bore hole refreezing rates.

2.2 Sea Ice and Freezing in Supercooled Seawater

Heat losses into the atmosphere and the variation of freezing point with depth and salinity are the primary controls on sea ice formation in Antarctic environments. Heat

---

[1]LAV location is not given in Bender and Gow (1961) but rather is taken from Hoinkes (1961).
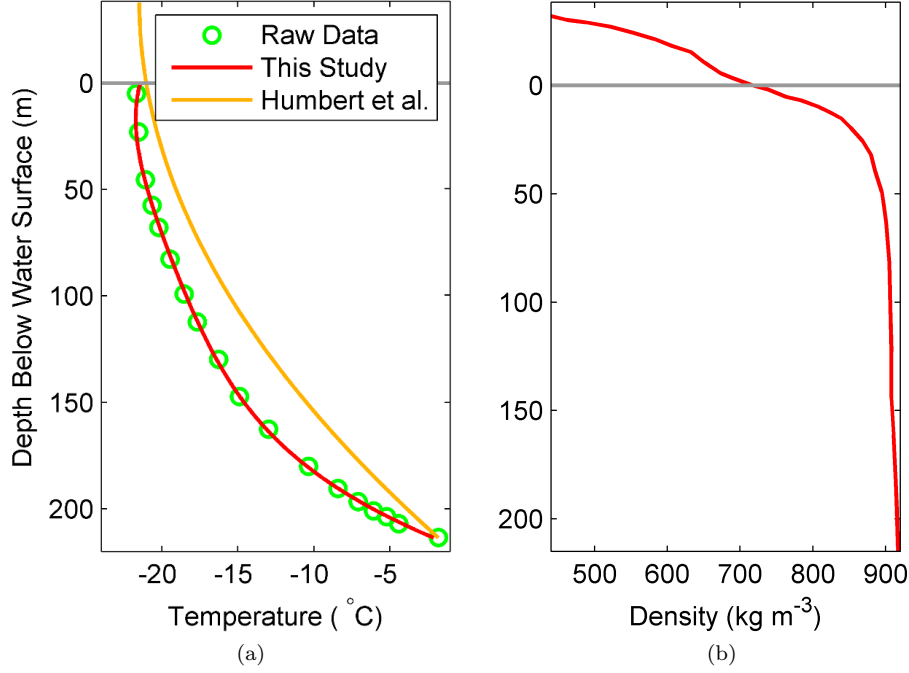
Figure 2.1: (a) Temperature profiles of the (vertically scaled) raw data reproduced from Bender and Gow (1961), the fit used for this study and the fit described by Humbert et al. (2005). (b) Density profile (vertically scaled). Depth is taken relative to the water level in the bore hole (see Section 3.2).

losses drive growth only at the surface, whereas supercooling of water can cause growth of crystals at depth in the ocean.

Sea ice first forms due to consolidation of crystals at the ocean surface due to heat loss into the surrounding air (Weeks, 2010). Heat loss continues as the ice grows by conduction through this layer of ice until it is about 2 m thick. Close to the ice shelves, the accumulation of crystals at the base is also an important factor in sea ice growth. The supercooling of water below the surface causes plate-like ice crystals to accumulate and fuse together into a porous structure known as the sub-ice platelet layer (Dempsey et al., 2010; Gough et al., under review).

Melting at the ice/water interface below an ice shelf acts to cool and dilute the surrounding seawater, creating Ice Shelf Water, which then rises due to buoyancy. A decrease in the freezing point accompanies the rise of the plume due to the decrease in pressure; the plume becomes supercooled in situ. The magnitude of the supercooling varies with season but it does not often exceed 20 mK, with this value being only a few times larger than the associated measurement error (Leonard et al., 2006). Ice crystals therefore grow in the rising water plume, this being known as frazil ice. Smaller crystals are kept in suspension by turbulence and subsequently transported out from beneath the ice shelf. Larger crystals become deposited at the base of the ice shelf. Consolidation of these crystals over time produces an open textured ice type at the base of the ice shelf called marine ice (Smedsrud and Jenkins, 2004). The overall mechanism is known as an ice pump.

There are two common traits shown by ice forming in seawater.

- Only a fraction of solid ice, ϕ, will be present in a given volume of the refrozen structure. The rest is composed of seawater/brine.

- The ice will tend to reject the dissolved salt from becoming incorporated into its structure during formation.

2.3   Oceanographic Techniques

A number of techniques taken from the field of oceanography will be used in this study. A short description of the relevant techniques is given here.

2.3.1   CTD Profilers

A CTD profiler is an instrument widely used in oceanography. Its purpose is to find salinity (S), calculated from electrical conductivity; temperature (T), measured directly and depth (z), calculated from hydrostatic pressure. The profiler used in this study takes measurements at a frequency of 4 Hz, effectively creating continuous, vertical profiles of salinity, temperature and pressure. By using an appropriate equation of state (see Appendix A) a number of other useful variables, such as density, freezing point, specific heat capacity and many more can be derived from the measurements.

The Practical Salinity Scale 1978, PSS-78, and the Equation of State for Seawater 1980, EOS-80 (UNESCO, 1980) used in this study have recently been superceded by the International Thermodynamic Equation of State of Seawater 2010, TEOS-10 (IOC et al.). The accuracy required in this thesis means that the UNESCO equation of state is indistinguishable from the most modern version.

The raw data from these was provided for this study. An outline of the process I used to treat this data is given in Appendix B. The specific instrument used in the field study was a Sea Bird Electronics SBE 19+ fitted with a SBE 38 oxygen sensor (details given in Appendix C).

2.3.2   Potential Density

The potential density is defined as the density attained by a fluid particle if taken isentropically to a standard pressure, here atmospheric pressure (Kundu and Cohen, 2002). It serves to remove the changes in density due to pressure variation and is the convention used by oceanographers to report measurements. The MatLab routine used in this study to calculate potential density from salinity, temperature and pressure values is given by Morgan (2003).

In this study density changes due to pressure variation will be small in comparison to changes due to salinity and temperature variation. Therefore, potential density and density can be treated as approximately equal.

2.3.3   Buoyancy Frequency

The buoyancy frequency (N), also known as the Brunt-Väisälä frequency, plays an important role in the study of stratified fluids and internal mixing.

It is defined by the equation

$$N^2 = -\frac{g}{\rho_0}\frac{d\rho}{dz} \tag{2.1}$$

where ρ is the potential density and ρ_0 is a constant reference density, i.e. the density at atmospheric pressure (Kundu and Cohen, 2002).

For a stably stratified fluid (positive N^2) it gives the frequency of oscillation of a vertically displaced fluid particle. A negative value of N^2 represents unstable stratification and in the upper ocean often implies overturning will occur. However, this may be affected by the boundaries imposed on the fluid (Batchelor and Nitsche, 1993) e.g. the sides of the bore hole.

2.3.4   Temperature – Salinity Diagrams

A T-S diagram is a scatter plot of salinity and temperature in which different water masses can be identified. A water mass is a body of water with distinct properties such as salinity, temperature and chemical composition. If the body of water were completely homogeneous then the T-S diagram will show a single point. When two water masses mix in a closed system the T-S diagram will show a straight line (Colling, 2001). This concept is important for this study because in a bore hole there are two end members, the fresh water at the top of the hole and the seawater below the hole. In this situation a straight line will represent an equilibrium.

Lines of constant density are often overlaid on T-S diagrams to give an indication of depth. Here a colour gradient will be used instead.

Chapter 3

Drilling in Ice Shelves

3.1   Process of Hot Water Drilling

A Hot Water Drill (HWD) is a tool used to provide access to remote regions under a thick layer of ice by melting an approximately cylindrical hole with hot, pressurised water. It is not uncommon for these drills to penetrate ice to depths greater than 1 km in cold ice (Tsutaki and Sugiyama, 2009; Engelhardt et al., 2000; Humphrey and Echelmeyer, 1990). Here attention will however be focused on the creation of a bore hole of large diameter (≈ 0.6 m) in the thin part of an ice shelf (≈ 250 m).

Creating a bore hole using a HWD is not a simple process. Although the fine details of the drilling procedures are not required for this study some background is needed as the time required to drill the hole is of importance in calculating a refreezing rate. For the hole involved in this study a three stage process was used. First a well was created, second a thin hole was drilled and last that hole was reamed to widen it to the desired diameter.

The time required to drill is dependent on many variables such as the thickness of the ice shelf, the temperature of the hot water, the required diameter, the properties of the hose and the vertical temperature profile in the ice.

Stage One - The Well

Initially, the hot water can be created only through melting snow collected from the surface and then heating it to the desired temperature of $85 - 90$ °C. The water must also be pressurised at the surface so as to provide sufficient flow at the nozzle. The pressures recorded during drilling ranged significantly but were of the order of tens of atmospheres. Naturally this requires a large input of energy; a simple calculation shows that approximately half of the energy input is required to effect the phase transition. Therefore it is beneficial to recycle the water as opposed to continually melting ice.

The first step, creating the well, involves drilling a hole significantly shorter than the thickness of the ice shelf; drilling is stopped a small distance below sea level[1]. It is created with the purpose of holding a significant amount of water allowing recirculation to the heater at the surface. Once the well is formed a submersible pump, connected by a hose to the surface, is lowered into it. A schematic of the well is given in Figure 3.1.

Stage Two - The Pilot Hole

A small diameter hole is drilled to establish a hydraulic connection to the ocean below. This hole is drilled sufficiently close to the well such that the main hole and well

---

[1]Sea level is of no significance until the second stage is completed.

effectively form a single large hole.

At the moment the drill bores through the ice shelf base an abrupt change in water pressure ensues. This occurs because the pressure at the base of the hole due to the height of water in the hole is larger than the surrounding pressure of the ocean. A significant movement of water out of the hole takes place ($\approx$ 5 m decrease in height in the present study). The ocean below now acts as a reservoir of salt and thermal energy.

Stage Three - Reaming the Hole

Enlarging the diameter is necessary for the hole to provide access for oceanographic instruments for a sustained period. The hole undergoes a process known as reaming. It is similar to the second stage, except a drilling attachment appropriate for enlarging diameter, as opposed to drilling downward, is employed. Reaming causes significant mixing because less dense water from the well is pumped throughout the hole which acts to distribute salt and thermal energy in a disordered manner, which tends to equilibrium thereafter. It is worth noting that hot water was being pumped from the reamer while being both lowered and raised.
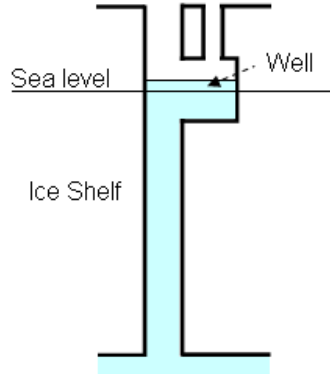
Figure 3.1: Connection of the well and the main bore hole (Not to scale).

At depth the water leaving the nozzle will be at a noticeably lower temperature than it was at the surface. This is due to heat being conducted radially outward from the hose at all points above the nozzle. Humphrey and Echelmeyer (1990) show that the temperature of water in the hose drops exponentially with depth; the characteristic decay length (depth at which $T = T_{surf}/e$) being approximately $500 - 1500$ m. Therefore heat loss out of the hose is not a large problem for a 250 m deep bore hole. A deeper hole would require the drill speed be slowed with depth to produce a hole of constant diameter. The rates of drilling can be estimated from Figure 3.2.

Necking, as described by Makinson (1993), is an important factor that a driller must bear in mind. This occurs when the diameter of the hole is greatly reduced at the base of an ice shelf because hot water escapes into the ocean rather than being used to melt ice. Necking is easily avoided by slowing the drilling rate near the base of the hole. Figure 3.2 does not clearly show the slower rate of drilling, however inspection of drilling records and video recordings through the hole show necking was avoided.
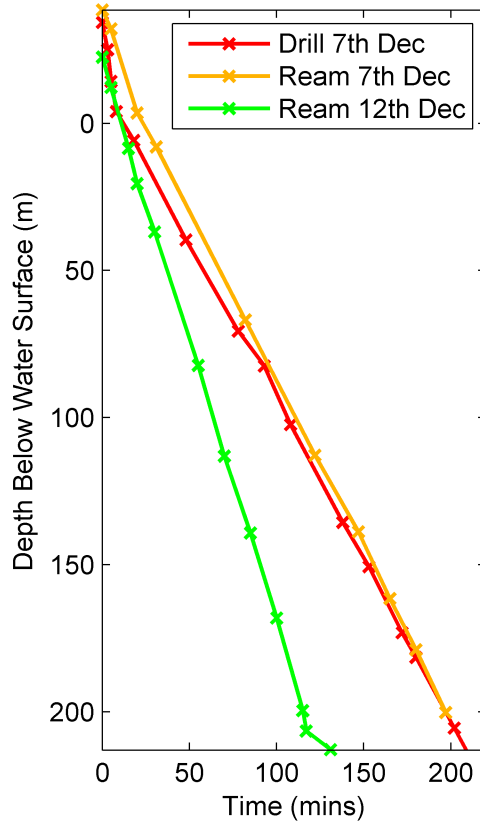
Figure 3.2: Depth of the HWD during descent for both drilling and reaming on the 7th and 12th of December. Only reaming of the hole was required on the 12th of December.

3.2 Bore Hole Properties

3.2.1 Water Surface Level

There are a number of possible schemes that could be used to specify lengths in the vertical direction. The most natural reference point, and the one to be used throughout this study, is the surface of water in the bore hole. This is distinctly different from both the surface of the ice shelf and the nominal sea level. The vertical axis is chosen to increase with depth, that is z is positive downwards.

The vertical lengths of interest are given in Figure 3.3 and explained in the paragraphs following. Specific numerical values for these lengths at the bore hole site were recorded and tabulated by M. Williams and C. Stewart and are given in Table 3.1.

Calculating Nominal Sea Level (NSL) involves assuming a standard density water at $T = 0°$C and $S = 35$ PSU which is very close to the mean density of seawater in the Southern Ocean. This density, along with a latitude dependent gravity, is used to determine the depth for any given pressure in the open ocean at the ice shelf front. The base of the ice shelf is identified by an abrupt change in potential density; the corresponding pressure measurement can then be used to find the depth of the base below NSL.

The most significant depth, that of the depth of water in the bore hole, is related to the cumulative summation of density values to the base of the shelf (see Appendix
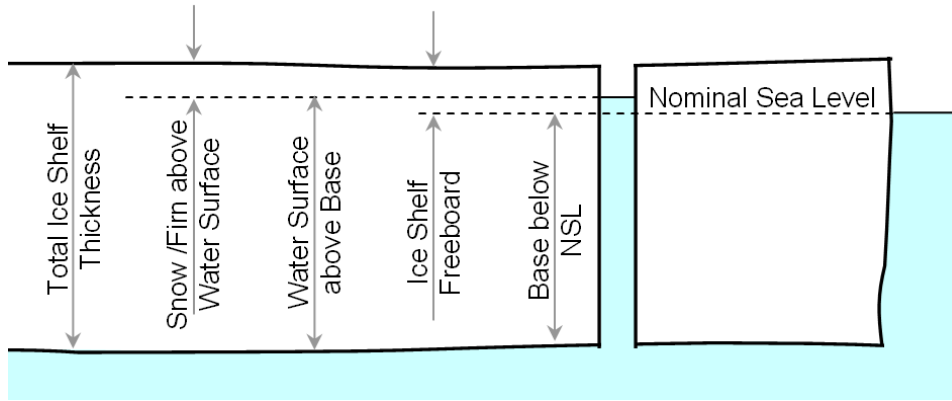
Figure 3.3: Cross-sectional view of an ice shelf showing the heights of significance. The well described in Section 3.1 is removed for clarity.

Table 3.1: Significant measurements at the bore hole site. Note: not all measurements are independent.

	Height (m)	Error (m)
Total Ice Shelf Thickness	252	1
Water Surface above Base	213.6	1
Snow/Firn above water surface	38.5	1
Ice Shelf Base below NSL	209	1
Water Level in Hole above NSL	4.6	0.1
Ice Shelf Freeboard	43.1	1

B for more detail). Values for density throughout the hole are determined from an equation of state (Appendix A) using CTD data as inputs. The total thickness of the ice shelf can then be found by adding to this the distance between the top of the ice shelf and the surface of the water. A float attached to a tape is lowered from the snow surface until the water surface is reached, allowing height to be recorded.

The main source of error is the measurement of the height of snow/firn above the water because over time the water in the hole will mix with the ocean below and naturally become more saline, hence denser, causing the difference between the water surface in the hole and NSL to decrease.

3.2.2 Uniformity

Unlike a mechanical drill a HWD cannot be expected to produce a perfectly uniform hole. The models presented later rely on the drilled hole being treated as a uniform cylinder. A short discussion of the validity of this assumption is given based on both video evidence from the hole and a separate example of a bore hole profile taken from Makinson (1993).

Video Evidence

Several videos were recorded to check the uniformity of the hole after reaming, amongst other purposes. The camera produced videos of minutes in length clearly showing the shape of the hole and the smoothness of the sides.

As the camera descended the video showed that the hole was smooth and approximately circular as desired. A rod of 400 mm in length was attached to the camera to

provide a scale to judge the diameter of the hole. I found it difficult to discern from the video the range over which the diameter changes with depth. The best estimate of hole size was chosen to be a constant diameter of 600 mm (personal communication, M. Williams).

Previous Studies

Makinson (1993) describes the direct caliper measurements of a holes diameter soon after a 540 m bore hole was drilled in the Ronne Ice Shelf. Figure 3.4 is duplicated from his paper.

Some care must be given to how Figure 3.4 is interpreted and applied to this study for several reasons:

- The paper describes a hole of smaller diameter, meaning the relative deviation with depth of the diameter from average could be expected to be larger for Makinson's study.

- The measurements were taken from a 1990/91 field study, implying breadth of knowledge of good drilling practices and access to tools required to produce a uniform hole would have been noticeably less in comparison to the 2010 NIWA field study.

- The aspect ratio of the figure should be considered as first inspection may suggest that the hole has a rather jagged surface.

- As described in 3.1 necking did not occur in the hole used in the present study.

- Makinson has used "cavity" in place of "well".

3.3 Expected Characteristics of Refrozen Ice

The growth of ice in a bore hole is not as well studied as other natural forms; the literature appears to contain nothing on its structure and formation mechanism. A bore hole is an artificial geometry unlike anything that could be found naturally. However, ice growth here should parallel that found in certain Antarctic environments. It is expected that the ice will freeze against the bore hole wall with a sparse, disordered structure. This is most similar to the growth of platelet ice and marine ice as both processes occur in saline conditions and involve the accumulation and growth of suspended crystals in supercooled water. An example of the structure that would be expected is shown in Figure 3.5.

Knowledge of the mechanism is important to this study for determining the solid fraction of ice (ϕ) that grows in a particular volume of seawater. The mechanism is effectively accounted for by this single parameter. A description of how its value is estimated is given in Chapter 5.

3.4 Measured Water Properties in the Bore Hole

Figures 3.6 – 3.11 show a number of the water properties measured and derived from measurements, across the two sets of 10 CTD casts.
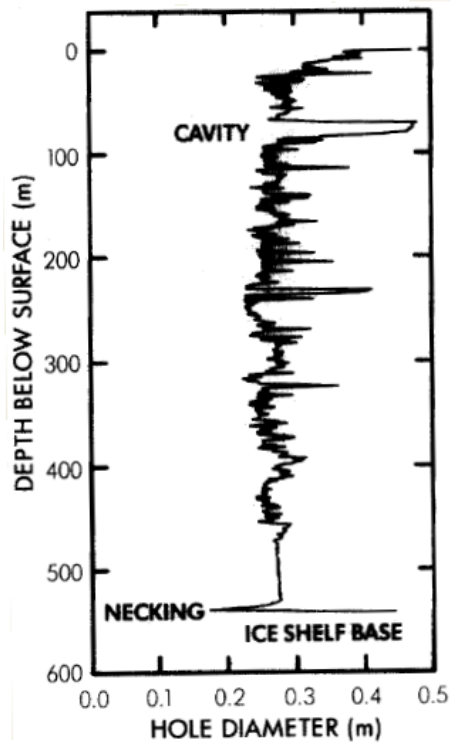
Figure 3.4: A bore hole diameter profile obtained soon after reaming of the hole. (Duplication of Figure 6 from Makinson (1993).)
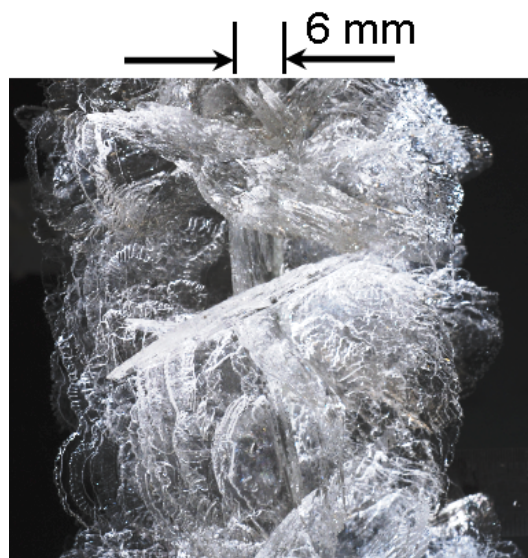
Figure 3.5: Ice that has formed on a mooring line suspended in the near surface ocean. Similar refrozen structures are expected inside the bore hole. Photo courtesy of C. Stevens (NIWA).
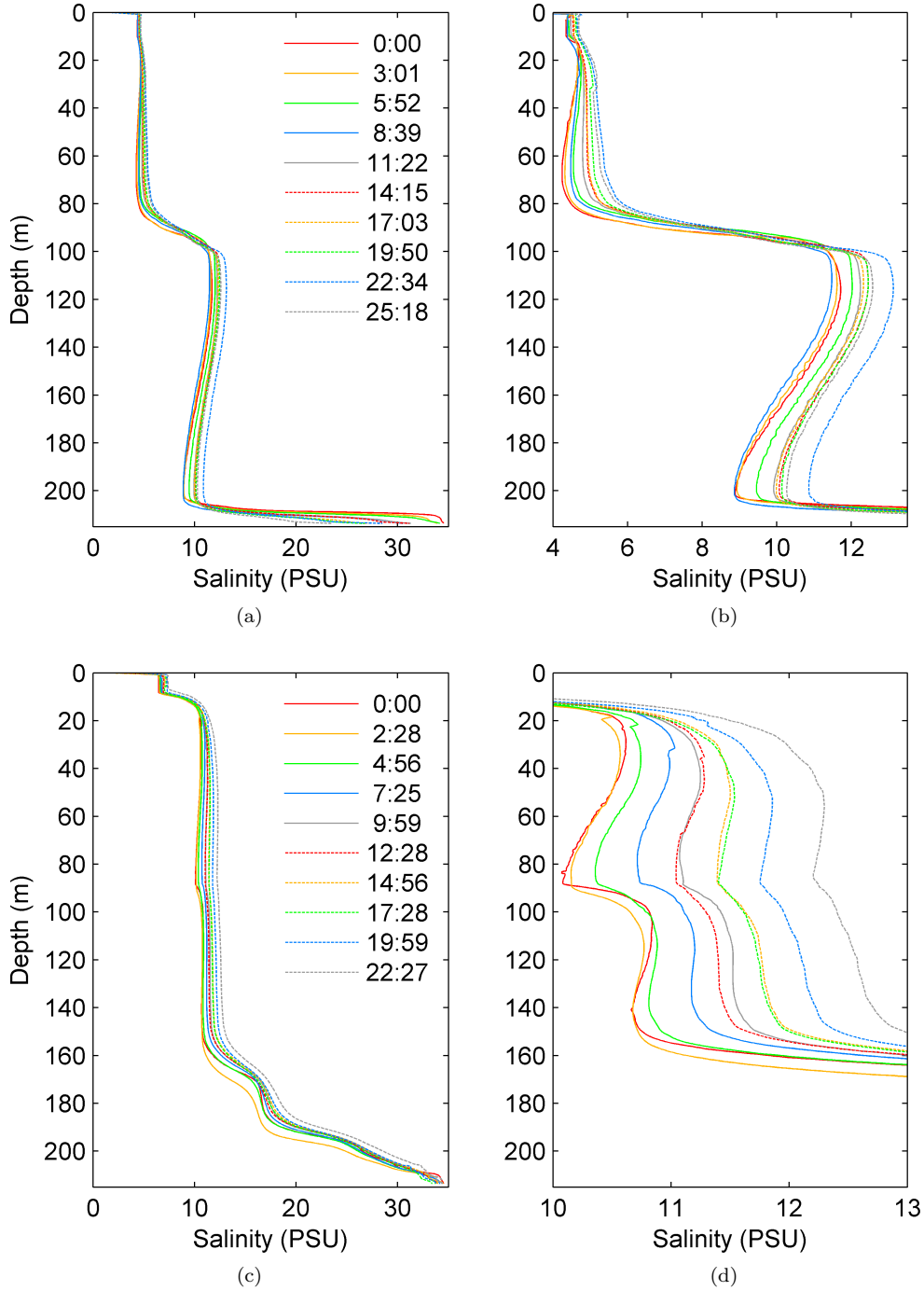
Figure 3.6: (a) and (c) The variation of salinity with time and depth for measurements taken on 8 − 9 December and 13 − 14 December respectively. (b) and (d) The same data sets with the regions of interest enlarged. The legends refer to the number of hours and minutes before each cast started relative to the first.

Salinity is much less than seawater beyond the ice shelf front (∼35 PSU) due to mixing of the melted ice shelf. The halocline at 80 − 100 m in (a/b) and the cusp in (c/d) are probably artefacts of drilling.

14
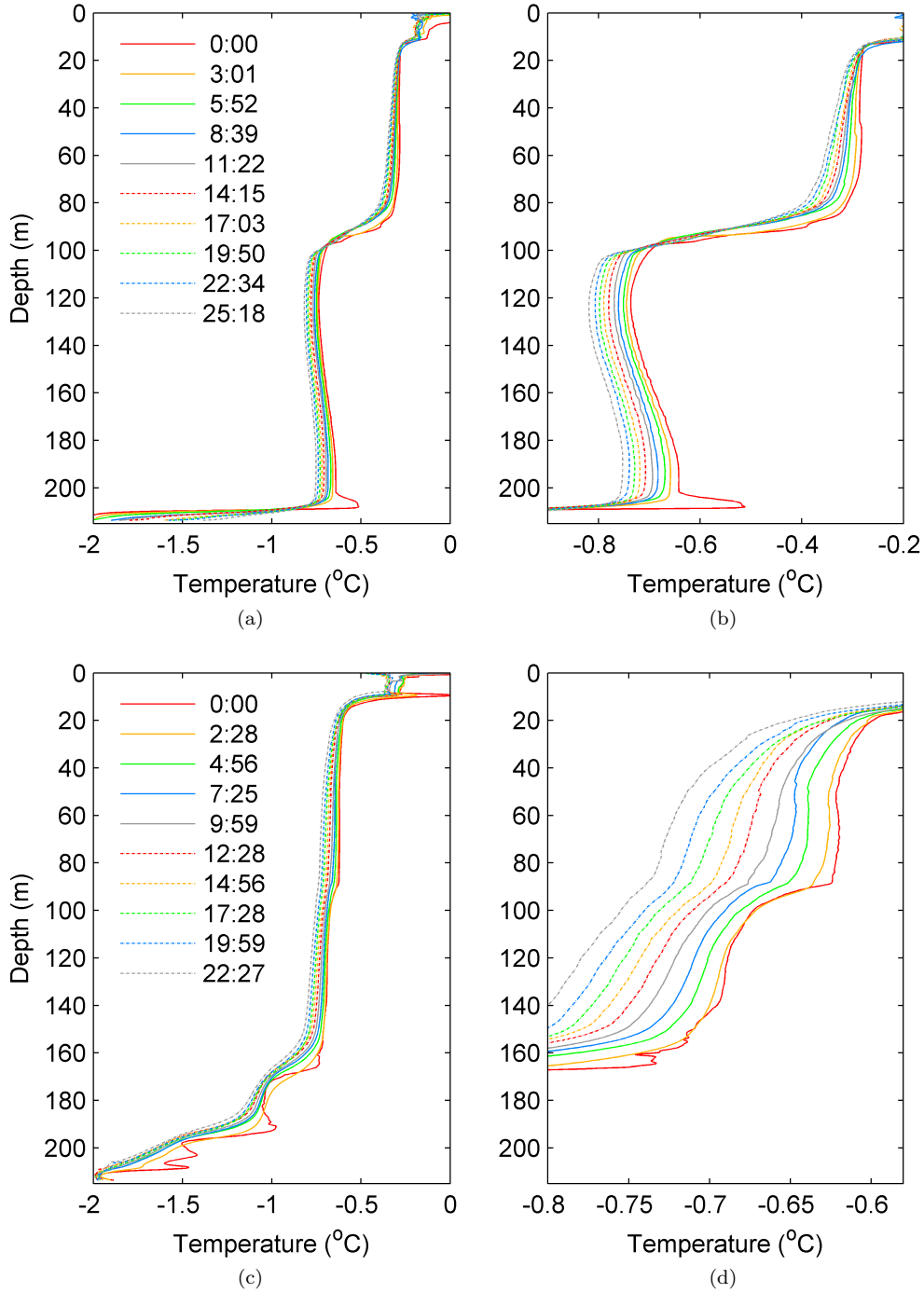
Figure 3.7: (a) and (c) The variation of temperature with time and depth for measurements taken on 8 − 9 of December and 13 − 14 December respectively. (b) and (d) The same data sets with the regions of interest enlarged. The legends refer to the number of hours and minutes before each cast started relative to the first.

The temperature is essentially determined by salinity as water in the hole is close to the freezing point (see Figure 3.8)
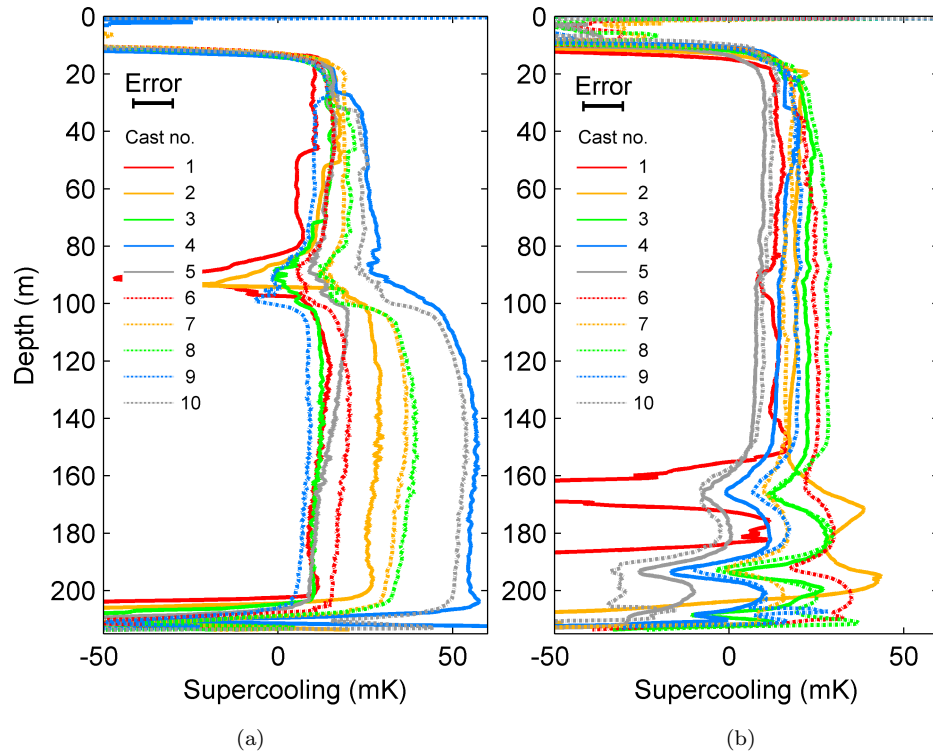
Figure 3.8: The variation of supercooling with depth for the 10 CTD casts taken on (a) 8 – 9 December (b) 13 – 14 December. Positive values indicate supercooling. The error associated with these measurements is shown in the top left corner of the plots. It arises due to the initial accuracy of 5 mK in the temperature measurements and an uncertainty in the equation of state for seawater (Leonard et al., 2006).

Nearly all plots show the water to be within approximately 30 mK of the freezing point throughout the experiment for all depths (ignoring the ends which are not closed).
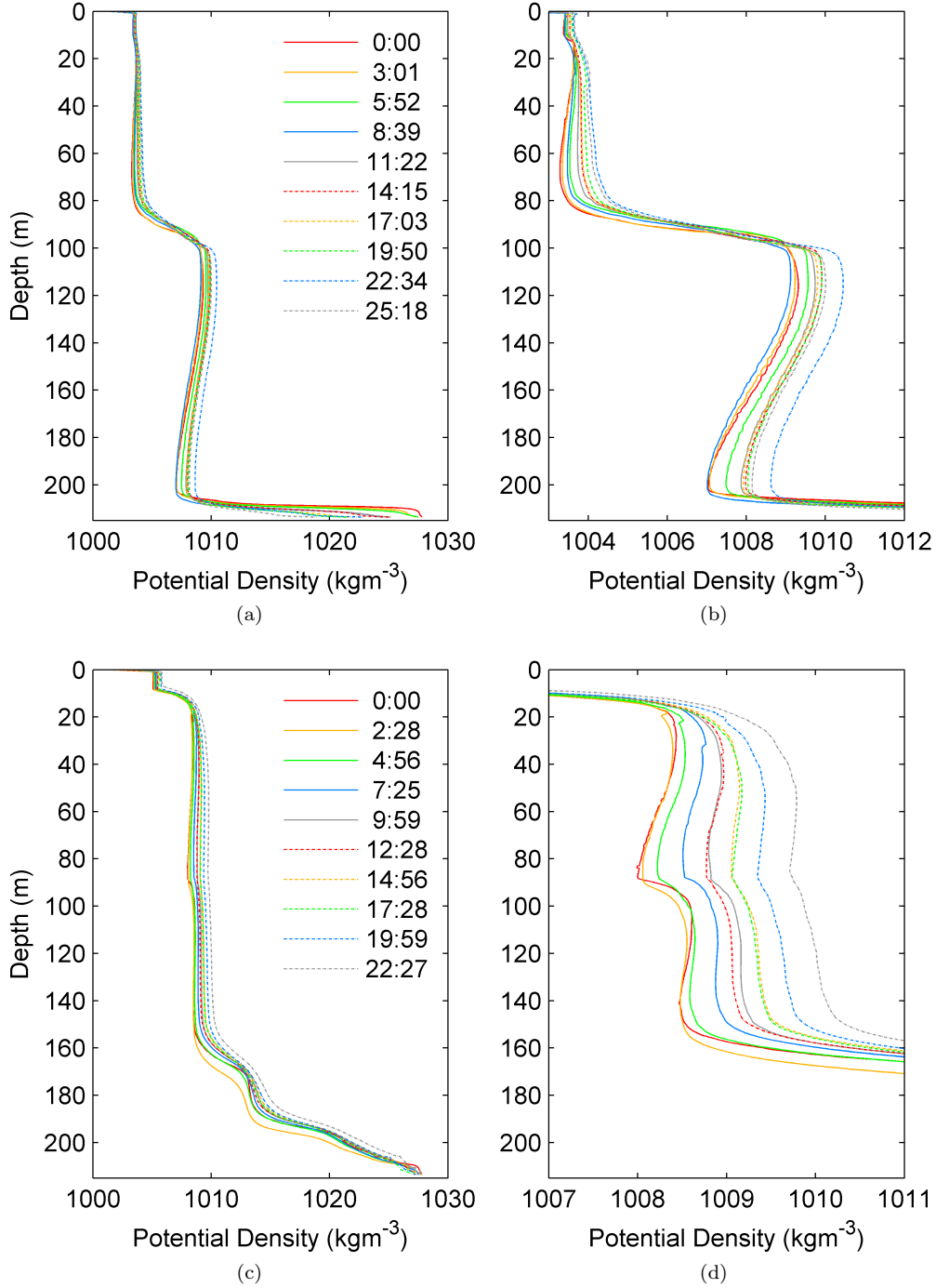
Figure 3.9: (a) and (c) The variation of potential density with time and depth for measurements taken on 8 − 9 of December and 13 − 14 December respectively. (b) and (d) The same data sets with the regions of interest enlarged. The legends refer to the number of hours and minutes before each cast started relative to the first.

Potential density shows hydrodynamical instability at a depth of 100 − 200 m in (a). The reason this is maintained is probably due to the geometry of the hole which requires that a critical Rayleigh number be exceeded for mixing to occur (Batchelor and Nitsche, 1993)

(a)

(b)
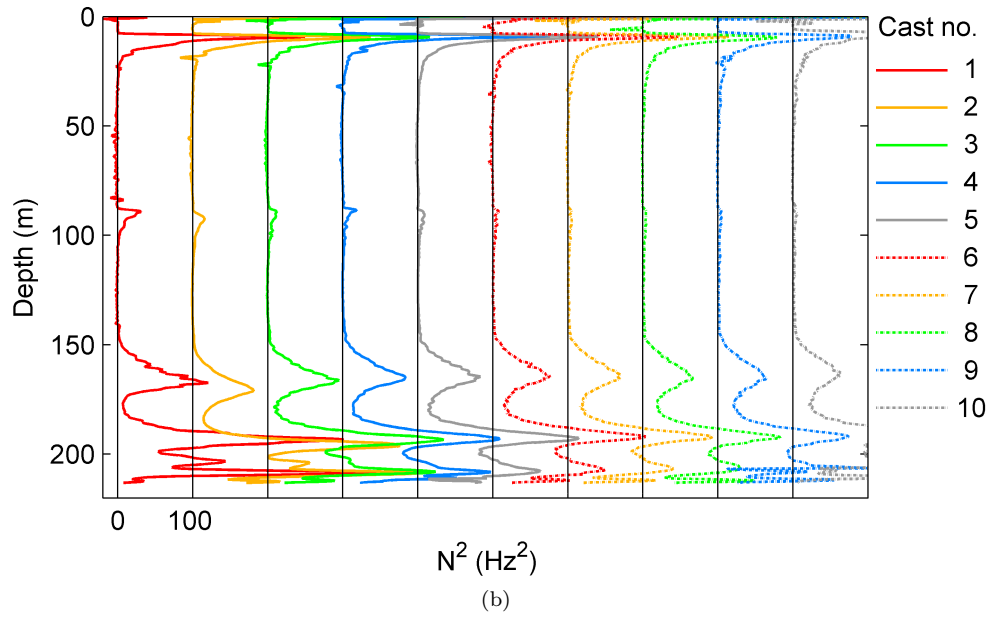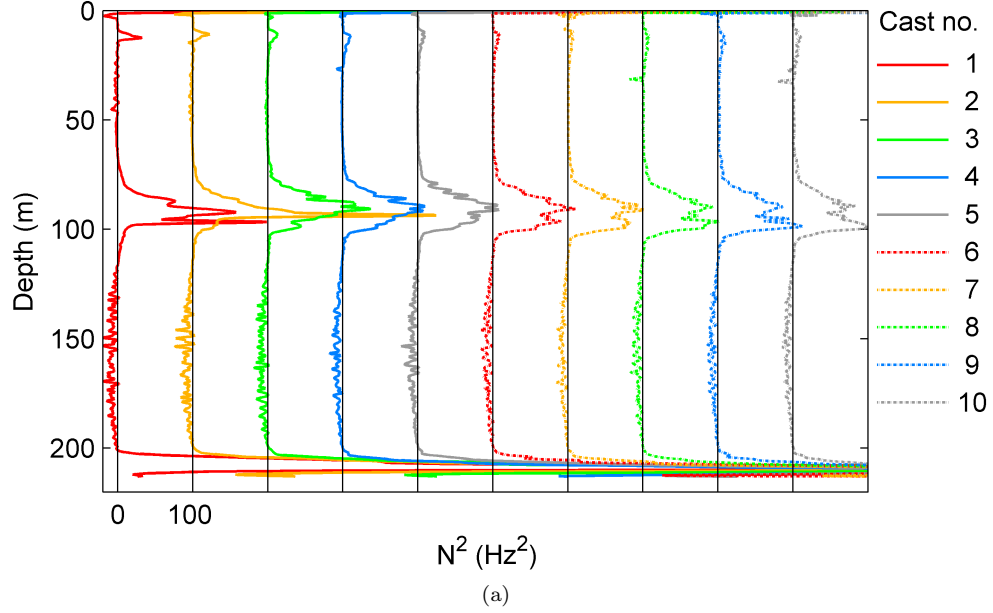
Figure 3.10: The variation of N^2 (where N is the buoyancy frequency) with depth for the 10 CTD casts taken on (a) 8 – 9 December (b) 13 – 14 December. Each cast is translated horizontally by $100\,\mathrm{Hz}^2$ from the last for clarity. The vertical lines show the respective zero values.

N^2 is negative for $100 - 200$ m in (a) but the constancy of the plots over time give evidence that no extensive amount of mixing is occuring.
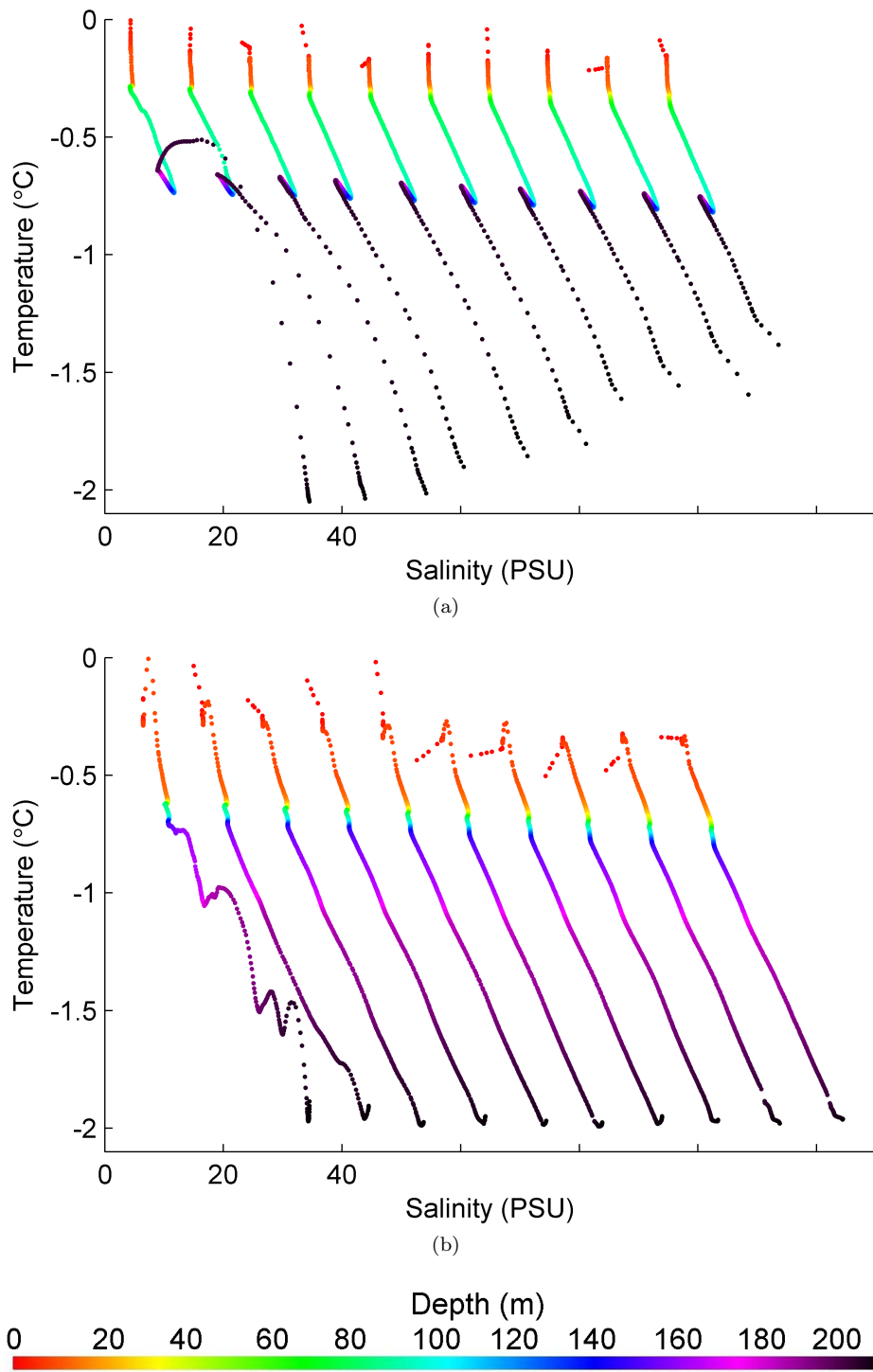
Figure 3.11: Temperature-Salinity diagrams for the 10 CTD casts taken on (a) $8 - 9$ December (b) $13 - 14$ December. Each cast is translated horizontally by 10 PSU from the last for clarity.

The two end members of the water in the bore hole can be identified at the top left (nearly fresh water at the surface) and the bottom right (seawater) of each plot.

Chapter 4

Radius Change from Salinity Measurements

4.1 Introduction

When ice forms in saline water the salt dissolved in the water tends to be rejected from the ice structure. A model based on this principle, and by assuming that the mass of salt in the hole is conserved, is to be developed here. CTD data sets will be used as the inputs allowing the closure of the hole to be modelled over the time measurements were being taken.

The definition of salinity has changed a number of times with the advent of increasingly accurate technology. The scale to be used in this study, PSS-78, defines salinity in terms of electrical conductivity. It is a unitless quantity, recorded in practical salinity units (PSU), in which the conductivity of seawater is measured relative to a standard solution of potassium chloride[1]. Appropriate algorithms are then used to find the salinity (UNESCO, 1980). The accuracy possible with this scale will not be needed. Instead we will work with the very close approximation that salinity is proportional to the mass fraction of salt in seawater. More precisely

$$S \approx 10^3 \frac{m_{\text{salt}}}{m_{\text{seawater}}} \qquad (4.1)$$

From this the mass of salt in a volume V of seawater with density ρ is $\rho V S$.

4.2 Salinity Variation

The salinity of water in the bore hole increases with time as the mass of salt in the hole stays approximately constant while the volume of water containing it decreases as ice grows. The purpose of this chapter is to use a geometric argument to relate the variation of salinity to the changing radius.

Seawater has a salinity of approximately 35 PSU. The average salinity in the hole is much lower as most of the water in the hole comes from the melted ice shelf which is fresh. The salt contained is primarily added by the mixing of ocean water into the hole caused by hot water drilling. The changes with salinity are shown in Figure 3.6 for the CTD casts taken on 8 – 9 December and 13 – 14 December.

The density of seawater is a function of temperature, salinity and pressure. Salinity will be the predominant factor at temperatures near the freezing point. Density values will also be required for this model. They are shown in Figure 3.9.

---

[1]The standard is an aqueous solution of KCl with a mass fraction of 32.4356 $\times 10^{-3}$ at one atmosphere at 15°C (UNESCO, 1980).

4.3 The Model

This model is based upon geometrical arguments, but requires a number of assumptions, the most important of which are listed below. The validity of each of these will be discussed in Section 4.6.

- There is no vertical movement of salt.

- The salinity is homogeneous in any given horizontal plane.

- The expansion of ice upon freezing from water is ignored.
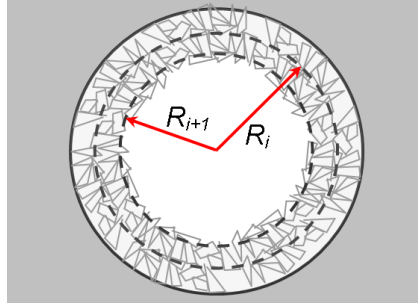
Figure 4.1: Cross-sectional view of the growth on the inside of the bore hole. The radius at time t_i is taken as the average radius of the diffuse interface. The shaded background represents the solid ice through which the hole was drilled, whilst the refrozen annulus has a smaller solid fraction. Crystals are not to scale.

The radius (R) will be calculated each time the CTD profiler descends. These times will be denoted t_i. Consider Figure 4.1. After a period of growth t_i becomes t_{i+1}, R_i becomes R_{i+1} and the salt that was originally spread evenly throughout the hole can be found in any one of three places.

- In the salt water contained in the now smaller hole.

- In the liquid fraction of the refrozen annulus.

- In the solid ice fraction of the refrozen annulus.

The model described here is based on the salt budget distributed through these three places.

4.4 Governing Equation

The variables that will be used in this model are listed in Table 4.1.

Conservation of mass of salt requires

$$\rho_i S_i V_i' = \rho_{i+1} S_{i+1} V_{i+1}' + \rho_{i+1} S_{i+1} A_i'(1 - \phi) + \rho_{ice} S_{ice} A_i' \phi \qquad (4.2)$$

The left hand side of the equation gives the total mass of salt per unit height inside the hole at time t_i. The first term on the right gives the mass of salt per unit height in the now smaller hole. The second term gives the mass of salt contained in the water fraction of the refrozen annulus per unit height at time t_{i+1}. The salinity of this is equal to the water in the hole because salinity is assumed homogeneous in any horizontal plane and the fraction solid is assumed low enough that the ice of the annulus is permeable. The last term gives the mass of salt per unit height contained in the solid ice fraction of the refrozen annulus.

Table 4.1: Variables used in the model of Chapter 4.

Symbol	Description
t_i	Times at which the hole radius is calculated (dictated by the times CTD profiles were taken)
R_i	Radius of hole at time t_i
ρ_i	Density of water at time t_i
S_i	Salinity of water at time t_i
V'_i	Volume per unit height of cylinder of radius R_i
A'_i	Volume per unit height of refrozen annulus grown between t_i and t_{i+1}
ϕ	Fraction of solid ice in the refrozen annulus
S_{ice}	Salinity of solid ice
ρ_{ice}	Density of solid ice
ΔR_i	$R_i - R_{i+1}$ (Positive for closure)

The bulk salinity of sea ice is due to brine trapped in mm-scale pockets spread throughout the pure ice structure. Here the refrozen annulus is assumed permeable, thus all the salt is assumed to be in the liquid. Hence, the last term disappears. This assumption may become invalid as the hole nears complete closure but this model treats early growth when salinity measurements were being taken.

Equation 4.2 is given in a form that shows conservation of salt explicitly. As both salinity and density are input variables we can find values for the radius at discrete time points. The relationship between R_{i+1} and R_i is derived from Equation 4.2 by using

$$V'_i = \pi R_i^2 \tag{4.3}$$

$$A'_i = \pi \left(R_i^2 - R_{i+1}^2 \right) \tag{4.4}$$

Therefore,

$$\rho_i S_i \pi R_i^2 = \rho_{i+1} S_{i+1} \pi R_{i+1}^2 + \rho_{i+1} S_{i+1} \pi (R_i^2 - R_{i+1}^2)(1 - \phi) \tag{4.5}$$

Solving Equation 4.5 for R_{i+1} gives

$$R_{i+1} = R_i \sqrt{\frac{\rho_i S_i - \rho_{i+1} S_{i+1}(1 - \phi)}{\rho_{i+1} S_{i+1} \phi}} \tag{4.6}$$

4.5 Results

Use of Equation 4.6, to predict closure rates, requires some care. It predicts that the decrease in radius between t_i and t_{i+1} is proportional to the current radius since R_{i+1}/R_i is equal to some constant (the square root term). This may seem unphysical upon first inspection; it would imply that the hole would reach complete closure at the same time irrespective of the initial radius. However, the variation of salinity with time would be expected to be non-linear. The volume of ice grown, and hence mass of salt rejected, is proportional to $2\pi R \Delta R$ whereas the mass of water it is added into is proportional to πR^2. As an example consider two extremes. The salt rejected from freezing on the side of a very large diameter hole would have little effect on the salinity because there is so much water for this rejected salt to move into. Conversely, if the hole were very narrow then for the same volume of ice growth the salinity should increase noticeably because of the smaller amount of water available to contain the added salt.

Therefore we need an estimate of the radius when $i = 0$, the point at which this model begins. The diameter at the time reaming finished was chosen in Section 3.2.2 to be 600 mm. By the time CTD measurements start this will have changed, and thus the value for R_0 is not well defined. Hence the results displayed here are in the non-dimensionalised form R/R_0 to emphasize that the values for radius should not be taken as absolute.

The iterative process used to implement Equation 4.6 is described in Appendix D. The result is shown in Figure 4.2
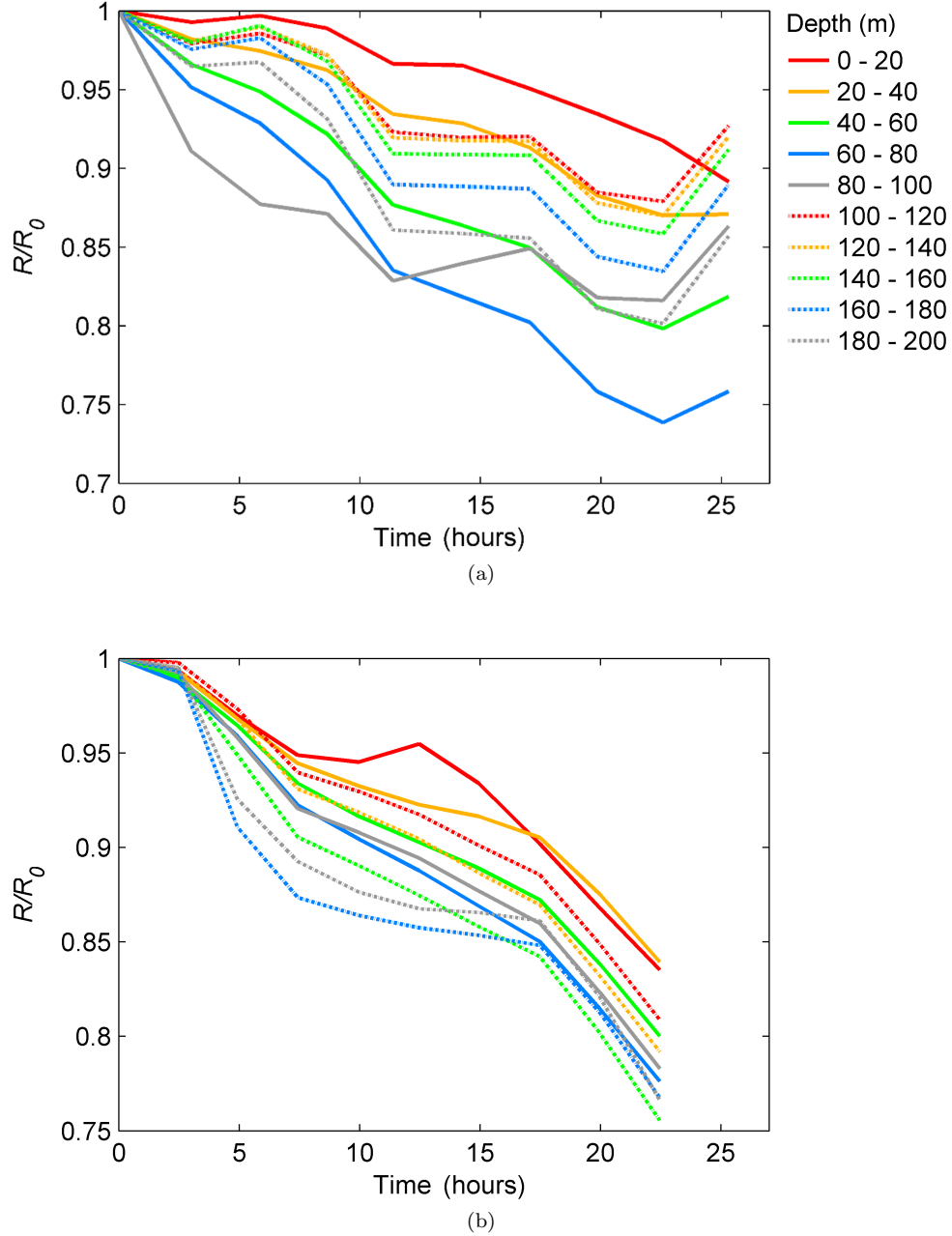
Figure 4.2: The closure of the radius predicted from salinity measurements on (a) $8 - 9$ December (b) $13 - 14$ December. The radius is shown in non-dimensionalised form and time is measured relative to when the model begins. ($\phi = 0.4$)

4.6 Validity of Model

The purpose of this section is to discuss the validity of the assumptions made in Section 4.3.

4.6.1 No vertical salt flux

Hot water drilling causes a large amount of mechanical mixing. After this finishes the mixing will be due only to movement of the CTD profiler and any instability in the water column. This model relies on a negligible flux of salt in the vertical direction. This assumption can be taken as reasonable provided the water is stably stratified. Quantifying the mixing or lack thereof is beyond the scope of this project but a few arguments will be given here to show mixing can be ignored.

Potential Density

The CTD measurements begun $16 - 18$ hours after the hole was reamed each time. This gave a significant amount of time for the water to relax toward a stably stratified state. Figure 4.3 shows that the sharp density gradients were reduced between the time of reaming and the time of the CTD casts beginning. Figure 4.3 uses data from a preliminary CTD cast taken only one hour after reaming was completed. Although the water between $100 - 200$ m appears to support a small unstable density gradient the constancy of the profiles (see Figures $3.6 - 3.10$) implies little large scale mixing. This mixing is suppressed by the geometry of the hole (Batchelor and Nitsche, 1993).
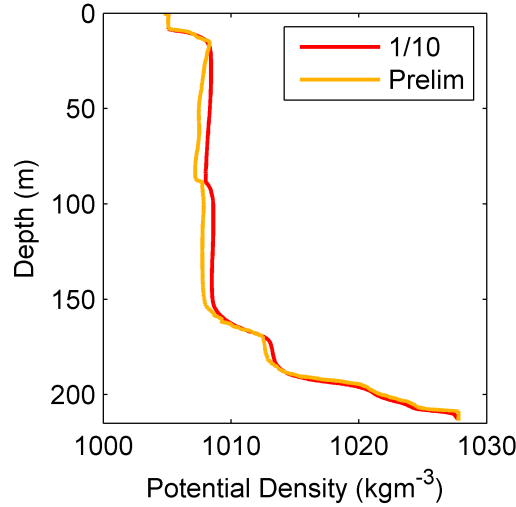
Figure 4.3: Potential density of the preliminary CTD cast taken one hour after reaming and the first of the 10 CTD casts taken on $13 - 14$ December (17.5 hours after reaming).

Buoyancy Frequency

Inspection of the plots of buoyancy frequency in Figure 3.10 show some regions of the water column have a positive N^2 value so the assumption of no vertical mixing is directly satisfied. Comparison of the plots shows that the $N^2 > 0$ requirement is satisfied over a large range of times and depths for the water measured on $13 - 14$ December. Therefore the refreezing predicted during this period could be expected to be more accurate in comparison to that of $8 - 9$ December which shows smaller regions where $N^2 > 0$.

24

The regions with a negative N^2 are unstable by definition. If this water column were in the ocean (i.e. unbounded) we would expect overturning. However, the use of buoyancy frequency to determine instability here becomes more complex due to the bounding of the water by a cylinder with a large aspect ratio (Batchelor and Nitsche, 1993).

Without a complete stability analysis the strongest argument of lack of mixing appears to be the remarkable constancy of the plots of 3.6 – 3.10 which implying a lack of mixing.

Overall we can still assume no vertical salt flux as it appears large scale mixing processes are not occuring, at least on time scales considered here.

4.6.2   Horizontal Salinity

This model relies on the salt being evenly distributed in any given horizontal plane. If the water were completely still then it could be expected that the water near the edges of the bore hole would have a higher salinity due to salt rejection upon freezing. However the freezing will cause mixing processes with small scales. Figure 4.4 shows an analogous result from a laboratory experiment. This was for a melting process in a stably stratified fluid but freezing can be expected to give a similar result (personal communication, M. Williams). The mathematical model of this spread of melt water into a series of layers is given by Huppert and Josberger (1980).

Along with mechanical mixing from the CTD profiler, this allows the assumption of the salinity being homogeneous across a horizontal slice of the bore hole to be valid.
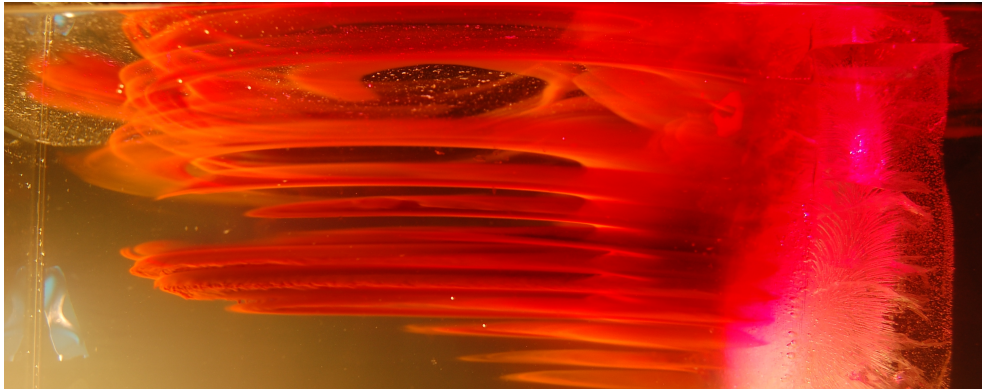
Figure 4.4: The movement of dye due to small scale mixing processes caused by ice melting in a stratified fluid. Photo courtesy of C. Stevens and N. Robinson (NIWA).

4.6.3   Volume Conservation

Solid ice is approximately $8 - 11\%$ less dense than the water in the bore hole. The model does not account for this change. It is ignored for two reasons. First, the ice shelf will float higher by a very small amount; this will occur to maintain hydrostatic equilibrium. Second, the total volume of ice that grows in the period of time considered in this model (the time between the first and last CTD cast) is a small fraction of the total volume of water in the hole.

Chapter 5

Radius Change from Heat Flux Considerations

5.1 Introduction

A model of the refreezing rate in a bore hole is developed. It takes into consideration the thermodynamic and geometric properties of the bore hole. The creation of such a model has been pursued a number of times in the literature; a review of these is given in Section 5.2.

The model is based upon two important physical principles; Fourier's law of heat conduction and the balance between the source of latent heat caused by freezing and the divergence of heat flux at the ice/water interface (Holland and Jenkins, 1999). The model involves three key steps. First, the temperature field in the ice outside the bore hole is determined as a function of depth, radial position and time. The need for a third spatial dimension is precluded as cylindrical symmetry is assumed. Second, the heat flux at the interface is ascertained. Last, the rate of ice growth is calculated.

For the model to be tractable and computationally efficient it is formulated by assuming the vertical temperature gradients in the water and in the surrounding ice are small enough that any heat flux in this direction can be considered negligible. This is justified as both the length and the time scales over which the vertical temperature changes are substantially longer than the corresponding scales in the horizontal direction.

The problem reduces to a large number of one dimensional problems in the radial direction only. The vertical variation through the ice shelf is accounted for by discretising all parameters that vary with depth. An exaggerated example of the process applied to the temperature profile in the ice shelf is shown in Figure 5.1.

5.2 Literature Review

The literature contains several works that model bore hole closure or treat the non-linear problem of a freezing interface moving in a radial direction. A variety of techniques from these articles provided inspiration and guidance for this study. The approach outlined in Section 5.1 differs from these models in a number of ways:

- the solid fraction described in Section 3.3 will be included.

- the model will incorporate the variation of a number of physical parameters with depth.
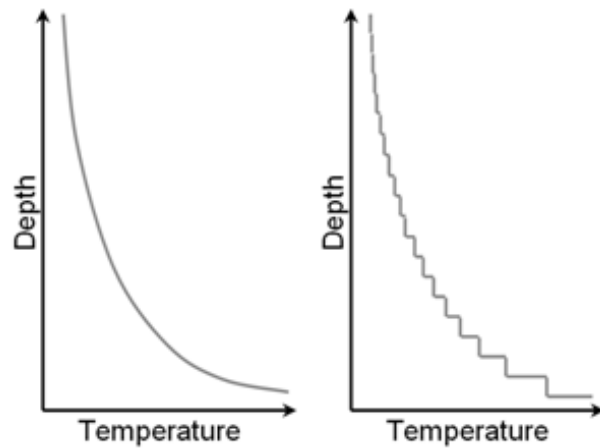
Figure 5.1: The continuous and discretised (exaggerated for clarity) temperature profiles through the ice shelf described in Section 2.1.2. The true grid with the constant spacing of 0.2 m would be indiscernible.

- the bore hole to be considered here is of larger diameter and smaller height than most holes specified in the literature.

- the model will treat closure of the hole both after initial drilling and after it has been kept open for an extended period.

The following is an overview of the papers which are most applicable to this study.

Humphrey and Echelmeyer (1990)

This paper describes a one dimensional finite element model that tracks the moving boundary of a refreezing bore hole. It is applied to two markedly different locations: Ice Stream B, Antarctica and Jackoshavns Isbrae, Greenland. These have temperatures that increase monotonically and decrease monotonically with depth respectively, thereby allowing the models to be adapted to a wide range of locations. The results are presented in a non-dimensionalised form to further their versatility. However the possibilities of a connection to the ocean or the presence of salt in the hole are precluded as both glaciers are situated over land.

When drilling deep holes (>1 km) the decrease in water temperature as it flows down the hose must be considered. Thus time spent drilling is incorporated into the refreezing model and the evolution of the radius is graphed for a range of heating times.

Napoleoni and Clarke (1978)

This paper presents the calculation of the refreezing of a 220 m bore hole with a minimum diameter of 3 cm. The hole is drilled for placing thermistor cables in the ice so need not stay open for an extended period. They treat the hose as a line source of heat and the resulting non-linear equation is solved via the finite difference method. Typical input values are chosen to produce dimensionalised results. A graph of hole closure with time is shown for seven likely ice temperatures.

Poots (1962)

This paper presents a mathematically rigorous approach to determining the location and time history of a solid-liquid interface with linear, cylindrical or spherical symmetry. They note that few exact analytical solutions to this problem, widely referred to

27

as a Stefan problem, exist. The solution they describe is that of approximate integral methods.

The time history of radial solidification for a circular cylinder is found but the mathematical complexity of the methods is beyond the scope of this study.

Kreith and Romie (1955)

This paper treats the inward freezing of an infinite cylinder in order to find the temperature-time history that must be applied at the boundary of the cylinder to produce a constant rate of travel of the solid-liquid interface. Their results show that a constant rate throughout is impossible because as the system nears complete closure the outer boundary must be raised above the freezing point, thereby melting the outside of the cylinder.

Harrison (1972)

This paper uses measurements of the hole closure rate to find the vertical temperature profile of a glacier. This rate, being much slower for temperate ice, can be measured by comparing the energy used by a thermal drill to the thickness of ice melted inside bore hole. The temperature profile in undisturbed ice can be derived from these measurements.

It is not comparable to this study but it is interesting to note the vastly smaller closure rate recorded for temperate ice. Averaged over depth, it was found to be 1.7 mm week^{-1} for a hole of 31 mm radius, drilled one week earlier. A hole in cold ice will close at a rate of the order of mm hour^{-1}.

Makinson (1993)

This paper does not attempt to model a freezing process. It is mentioned in this section as it includes direct measurements of closure rates for a bore hole in the Ronne Ice Shelf. The results recorded will be used in Section 5.8 to provide an estimate of the solid ice fraction. There is value in comparing the model of this chapter to the direct measurements from Makinson (1993) for two reasons:

- the refreezing rate was measured in an Antarctic ice shelf at a latitude very close to that of the RIS bore hole site.

- the hot water drilling process he outlines is very similar to the process described in Section 3.1 used for the NIWA study.

5.3 Variation of Parameters with Depth

There are seven parameters, listed in Table 5.1, that this model must contain; describing their variation with depth is the purpose of this section. All values stated in this section were taken from the CRC Handbook of Chemistry and Physics (Haynes, 2010).

Water Temperature

T_0 is one of two boundary conditions required for this model. It refers to the temperature of the water in the bore hole. It is known from CTD measurements to change very slowly with time; a typical change over the period of one day is 0.1°C.

A time dependent boundary condition could be incorporated into the model, however, the water temperature in the hole is not known over the entire closure period. The simplest approach is to allow T_0 to vary with respect to depth but be kept constant with respect to time. This is justified as the more important quanity, $T_0 - T_{ice}$, is tens

Table 5.1: Description, symbol and unit of each of the important parameters to be used throughout Chapter 5.

Parameter	Symbol	Units
Temperature (Water)	T_0	°C
Temperature (Ice)	T_{ice}	°C
Initial Radius	a	m
Density (Ice)	ρ	kgm^{-3}
Thermal Conductivity (Ice)	K	$\text{Wm}^{-1}\text{K}^{-1}$
Specific Heat Capacity (Ice)	c	$\text{Jkg}^{-1}\text{K}^{-1}$
Thermal Diffusivity (Ice)	κ	m^2s^{-1}

to hundreds of times larger than the variation of T_0 with time. Therefore T_0 will be taken as the time average of the temperatures recorded over the 10 CTD casts. The result is shown in Figure 5.2 for both sets of CTD casts.
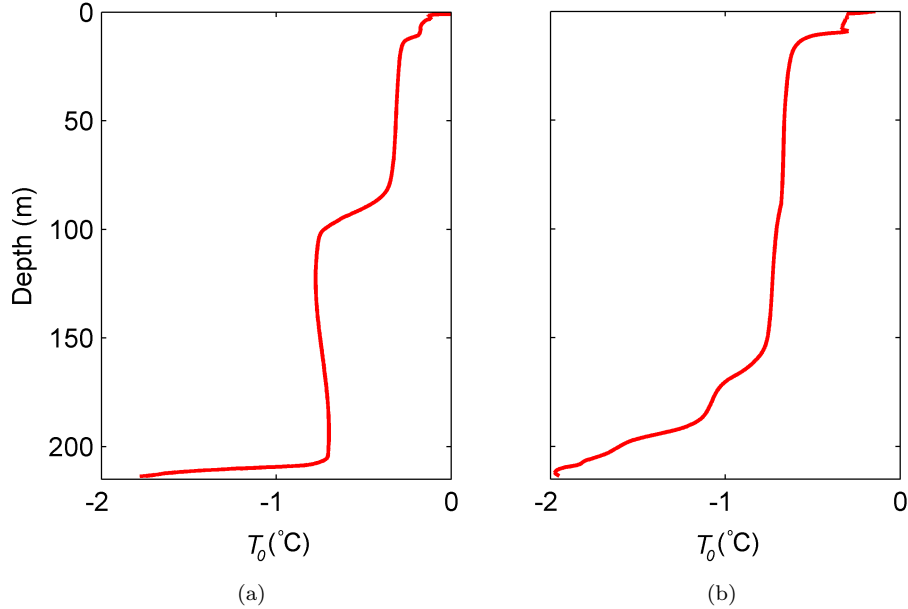
Figure 5.2: The prescribed function of T_0 with depth for (a) 8 – 9 December and (b) 13 – 14 December. The difference in profiles can be attributed to the mixing that occurs due to reaming between the two dates.

Ice Temperature

T_{ice} is the other of the two boundary conditions. It refers to the variation with depth of the temperature in the ice shelf at a large distance from the hole. The temperature must tend to T_{ice} as the radial position gets very large. The function modelling T_{ice} was previously discussed in Section 2.1.2.

Initial Radius

The initial radius is taken to be independent of depth (Section 3.2.2) and will be discussed no further in this section.

Density

The variation of density with depth was described in Section 2.1.3. It is mentioned here again as both thermal conductivity and thermal diffusivity are dependent on it.

It is worth noting that the density of solid ice containing no air is a weak function of temperature. It varies by less than 0.5% in the temperature range of interest (Haynes, 2010). The value of density for pure ice is taken as 917 kgm^{-3}.

Thermal Conductivity (Ice)

The thermal conductivity of any material is a function of structure and temperature. This study will work with values measured from the common, hexagonal form of ice and assume its structure is dependent only on density.

There is an approximately linear relationship between temperature and thermal conductivity over the range of temperatures encountered in an ice shelf. Representative values are given in Table 5.2.

Table 5.2: The thermal conductivity of ice (1h structure at 100 kPa) and specific heat capacity of ice (constant pressure) at representative temperatures. Linear interpolation provides intermediate values.

Temperature (°C)	Thermal Conductivity (Wm^{-1}K^{-1})	Specific Heat Capacity (J kg^{-1} K^{-1})
0	2.16	2.10
-10	2.26	2.02
-20	2.38	1.95
-30	2.50	1.88

An approach taken from Schwerdtfeger (1963) is used to account for changes with density. Although his paper concerns the thermal properties of sea ice he provides a means for calculating the thermal conductivity of bubbly, pure ice of any density. Equations 5.1 and 5.2 are replicated from his paper.

The model assumes all air trapped in the ice is contained in spherical bubbles. This is a definite simplification of the structure, especially in the low density sections of ice, yet a more sophisticated model is beyond the scope of this study. The purpose of using the simple model is to get a quantitative indication of how density affects thermal conductivity. The qualitative result is easily assumed; the air bubbles will reduce the rate of heat transfer thereby the thermal conductivity decreases.

The volume of air contained in unit volume of ice is

$$v = 1 - \frac{\rho_{bi}}{\rho_i} \tag{5.1}$$

where ρ_{bi} and ρ_i are the densities of bubbly and pure ice respectively.

The thermal conductivity of the bubbly ice is then given by

$$K_{bi} = \frac{2K_i + K_a - 2v(K_i - K_a)}{2K_i + K_a + v(K_i - K_a)} K_i \tag{5.2}$$

where K_i for ice is found from interpolation of the values of Table 5.2 and K_a for air is found from the equivalent process (values not shown).

Applying Equation 5.2 to the density-depth curve gives the thermal conductivity with depth as shown in Figure 5.3a.
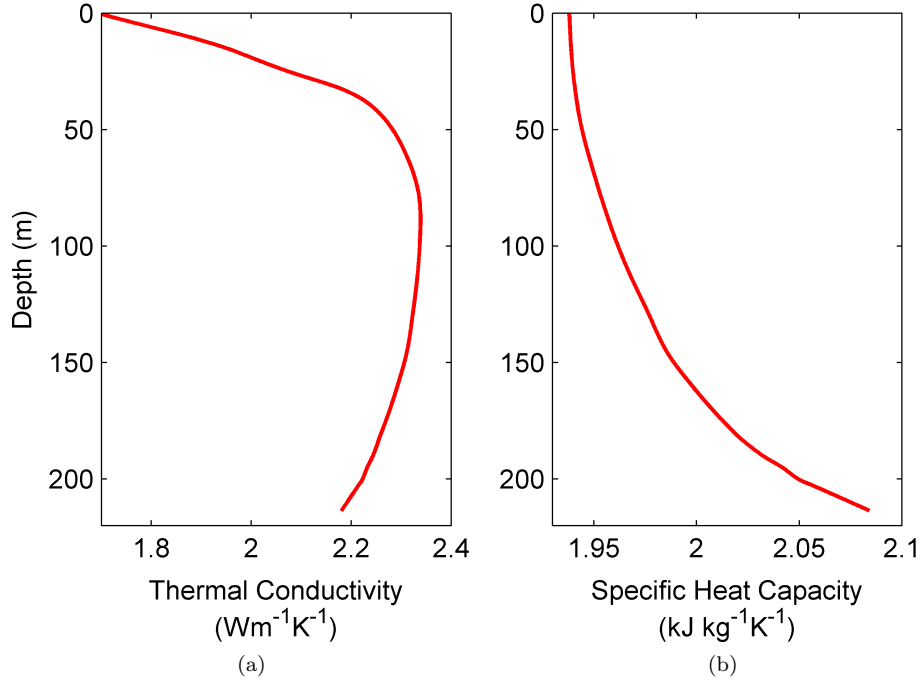
Figure 5.3: (a) The variation of thermal conductivity with depth. The dominant effect in the top region is the change in density, whereas temperature is the main factor in the lower half. (b) The variation of specific heat capacity with depth.

Specific Heat capacity (Ice)

The only change of specific heat capacity with depth that will be considered is that due to its small variation with temperature. Density has no effect as specific heat is independent of the mass of ice. As with thermal conductivity, it varies approximately linearly over the range of temperatures of interest. Its value increases by 8% between the temperatures at the top and bottom of the ice shelf respectively. Representative values of specific heat capacity (at constant pressure) of ice are given in Table 5.2. The specific heat at all depths is shown in Figure 5.3b.

Incorporating the variation of specific heat as the the surrounding ice warms up would add significant complexity to the code and will not be treated here.

Thermal Diffusivity (Ice)

The thermal diffusivity is an important quantity as it arises in the heat equation. It is essentially a measure of how quickly a material adjusts to the surrounding temperature. It is dependent on three previous parameters by the relation

$$\kappa = \frac{K}{\rho c}$$

Therefore calculating the variation of thermal diffusivity with depth is now straightforward. The appropriate K is K_{bi} from Equation 5.2. The result is shown in Figure 5.4.
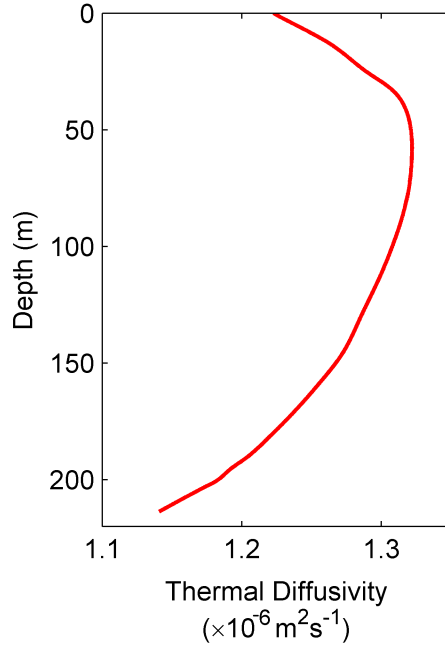
Figure 5.4: The variation of thermal diffusivity with depth.

5.4 The Heat Equation

A bore hole contains water very near its freezing temperature surrounded by ice at a lower temperature. This causes heat transfer across the interface. The purpose of this section is an application of Fourier's law of heat conduction to evaluate the temperature distribution in the surrounding ice.

5.4.1 The Mathematical Model

The bore hole is modelled as a cylinder composed of a large number of adjoining disks. The neglect of any vertical variation across the individual disks (Section 5.1) causes each one to be mathematically equivalent to an infinitely long cylinder. We require the temperature of the ice in the region $r \geq a$, as a function of radial position and time.

The following formulation is adapted from Carslaw and Jaeger (1959).

The Partial Differential Equation

In the ice there is no heat source so the conduction of heat is governed by

$$\nabla^2 T = \frac{1}{\kappa} \frac{\partial T}{\partial t} \tag{5.3}$$

when ice is assumped to be isotropic.

In cylindrical polar co-ordinates, with temperature independent of θ and z, this becomes

$$\frac{\partial^2 T}{\partial r^2} + \frac{1}{r} \frac{\partial T}{\partial r} = \frac{1}{\kappa} \frac{\partial T}{\partial t} \tag{5.4}$$

The Boundary Conditions

Two boundary conditions are required. First, the temperature at the surface $r = a$ is kept at the constant value of T_0. Second, as r becomes very large the temperature

32

tends to T_{ice}. Both T_0 and T_{ice} vary with depth but are single valued in each horizontal plane.

The Initial Condition

The actual initial condition is not straightforward and will be described later in Section 5.6. As a first step we consider the simplest initial condition in which the temperature of the ice at $t = 0$ is T_{ice} everywhere. This implies the bore hole was somehow instantaneously placed in the ice shelf. In spite of the simplification the final model will rely on results obtained from this method.

5.4.2 The Solution

Analytical Solution

Carslaw and Jaeger (1959) find the analytical solution using Laplace transforms. After the appropriate scaling and shift of their non-dimensionalised solution it becomes

$$T(r,t) = T_0 + \frac{2(T_0 - T_{ice})}{\pi} \int_0^\infty e^{-\kappa t u^2} \left(\frac{J_0(ur)Y_0(ua) - Y_0(ur)J_0(ua)}{J_0{}^2(ua) + Y_0{}^2(ua)} \right) \frac{du}{u} \quad (5.5)$$

where J_0 and Y_0 are Bessel functions of the first and second kind respectively.

Carslaw and Jaeger (1959) give series expansions of Equation 5.5 for small and large values of t but neither regime is applicable to this study. Applying numerical integration is also a challenge due to the singularity of the integrand at zero. This can be resolved using asymptotic expansions of Bessel functions as described by Goldenberg (1956) but will not be pursued here.

Numerical Solution

A numerical solution to Equation 5.4 was found as it was more suitable for extension to non-ideal conditions than the analytical solution. The partial differential equation (PDE) was handled with the built-in MatLab routine `pdepe` (MathWorks Inc., 2008). The implementation is discussed in Appendix E.

Carslaw and Jaeger (1959) graph the non-dimensionalised solution for temperature against radius for 10 representative times. This graph was reproduced from the numerical solution as a check for coding accuracy. Both graphs are shown in Figure 5.5.

5.5 Heat Fluxes

5.5.1 Heat Sources

There are three sources/sinks of heat in this model; the latent heat of freezing, the hot water drilling and the ocean.

Heat from the Ocean

Of the three sources, heat from the ocean is the most difficult to quantify. It is assumed negligible because CTD profiles in the hole (Section 3.4) show water temperature near the base varies significantly with depth but not with time.
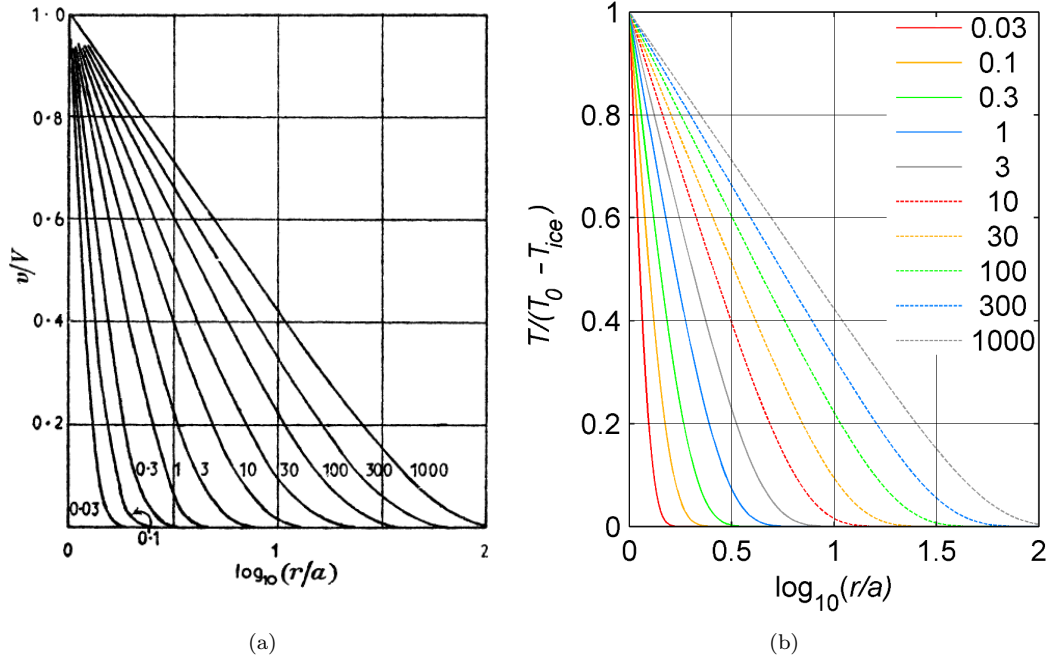
Figure 5.5: (a) Temperatures in the region bounded internally by a cylinder $r = a$ with zero initial temperature and constant surface temperature V. Duplicated from Figure 41 of Carslaw and Jaeger (1959). (b) Temperatures for the same region at an initial temperature T_{ice} and constant surface temperature T_0. Both vertical axes are equivalent with (a) being a special case of (b). The numbers shown on the graphs are non-dimensionalised times ($\kappa t/a^2$).

Heat from Hot Water Drilling

The thermal energy of the hot water is easily accounted for; the water temperature continues to drop until it reaches the freezing point. The time this takes to occur is estimated by Humphrey and Echelmeyer (1990). They state that during drilling it can be expected that at distances tens of metres above the nozzle all heat delivered to the tip is utilised in melting ice. Therefore it is reasonable to ignore the time taken to reach equilibrium.

This source of heat will help determine the appropriate initial conditions described in Section 5.6.

Latent Heat

Heat is released in the process of freezing. The source of latent heat will be distributed throughout the annular region of refrozen ice. The details of the refrozen ice structure are not known (Section 3.3) so instead the source will be assumed to be situated at the inner radius of the refreezing ice.

5.5.2   Heat Flux Balance

In the previous section it was shown that, after drilling, latent heat is the only heat source to consider. This allows a simple heat flux balance to be applied. At the interface the latent heat is equal to the sum of the sensible heats of the water and ice. In terms of fluxes

$$f_w + f_i = f_{latent} \tag{5.6}$$

34

f_w, the heat flux into the water, is assumed negliglible as the water changes temperature only very slowly (Section 5.3). f_i, the heat flux into the ice, is calculated from the temperature distribution described in Section 5.4.2. f_{latent} is the flux from released latent heat .

Therefore, by assumption, the quantity directly related to ice growth (f_{latent}) is known once f_i is known. For a volume V of water in which a fraction ϕ solidifies the latent heat released is $\rho\phi V L_f$ where $L_f = 3.34 \times 10^5$ Jkg^{-1}K^{-1} (Haynes, 2010). Applying this result to a cylinder of arbitrary height Δz and radius a gives the flux balance at the surface.

$$f_{latent} = f_i = \phi\rho L_f \frac{dV}{dt}\frac{1}{2\pi a\Delta z} \tag{5.7}$$

5.5.3 Heat Transfer in the Refrozen Ice

For conduction through a cylindrical surface, $r = a$, the heat flux is given by

$$f = -K\left[\frac{\partial T}{\partial r}\right]_{r=a} \tag{5.8}$$

Application of Equation 5.8 is accurate for small values of time when the moving radius is approximately equal to the fixed, initial radius, a. The inwardly moving radius will be explicitly denoted R to avoid any confusion with radial position r. Over time the layer of warm, refrozen ice will grow changing R significantly. An argument will now be given to show that the heat transferred through the fixed radius a is approximately the same as would be found from evaluating Equation 5.8 with R. The purpose of the argument is to ignore the need for the complex details of heat transfer in the refrozen ice.

As described in Section 3.3, the ice that grows is porous and the liquid fraction is assumed interconnected[1]. This allows convection to occur resulting in a significantly greater rate of heat transfer in comparison to conduction in the original ice. The effective thermal conductivity of the new ice will be denoted K_{eff}. Consider Figure 5.6, the heat flux must be continuous at the $r = a$ because no heat sources exist here.

$$-K_{eff}\left[\frac{\partial T}{\partial r}\right]_{r\rightarrow a^-} = -K_{ice}\left[\frac{\partial T}{\partial r}\right]_{r\rightarrow a^+} \tag{5.9}$$
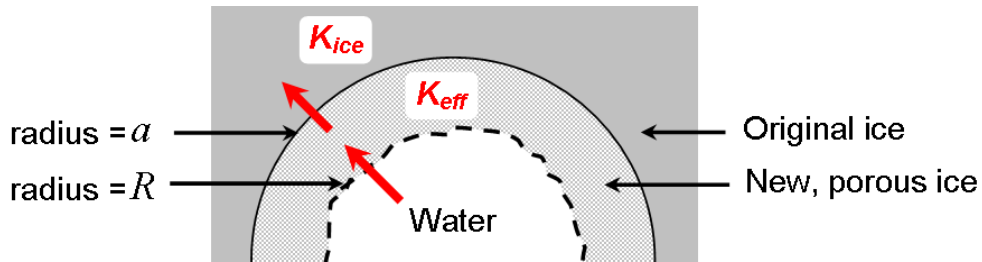
Figure 5.6: Cross-sectional view of half of the bore hole showing the different regions of ice and water and their respective thermal conductivities. A red arrows represent a heat flux across the surface.

Because $K_{eff} >> K_{ice}$ the temperature gradient inside of the boundary must be much smaller than it is outside. The large value of K_{eff} will mean that the refreezing ice is in a pseudo steady state because it takes longer for the ice to grow compared to

---

[1]This same assumption was used in a sophisticated model of refreezing sea ice cracks (Petrich et al., 2007) of similar width scale.

the time to reach an equilibrium temperature distribution. The general solution to the temperature distribution in the annulus is given by Carslaw and Jaeger (1959).

$$T(r) = A + Bln(r) \tag{5.10}$$

where A and B can be found from the fixed boundary temperatures.

The expected temperature field is represented in Figure 5.7.
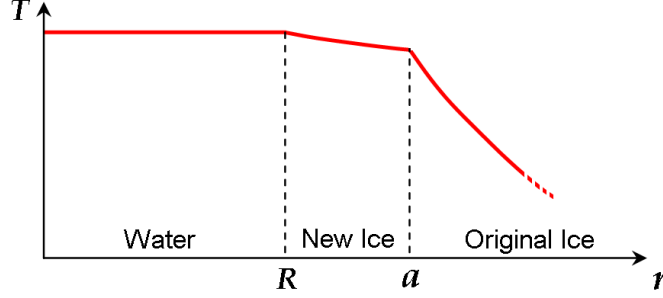
Figure 5.7: Expected temperature distribution in the water, new ice and original ice.

There is further justification for this expectation from an alternative context, the platelet layer at the base of sea ice. This also has a sparse, porous strucuture and a similar size scale. Gough et al. (under review) state that temperature measurements in the platelet layer are the same within measurement error as ocean measurements a few metres from the ice.

From here on all the points $r < a$ will be treated as isothermal (equal to T_0). This will become invalid for small values of R/a but by this stage the hole will be too small for oceanographic equipment and the closure rate calculated need not be as accurate.

5.5.4 Heat Flux into the Surrounding Ice

Equation 5.8 provides a means of calculating heat flux by using the value of the temperature gradient at a single point, $r = a$. This is inappropriate when using a numerical solution as the accuracy of the derivate at the boundary is limited. An alternative method is described below.

The total amount of heat that has diffused into the ice is given by

$$Q(t) = c \int_{\text{all ice}} \Delta T(r,t) dm \tag{5.11}$$

$$\Delta T(r,t) = T(r,t) - T(r,0) \tag{5.12}$$

An arbitrary height, Δz, is required to express the infinitesimal mass in cylindrical co-ordinates. It becomes

$$dm = 2\pi \, \rho \, \Delta z \, r dr \tag{5.13}$$

The heat flux, defined as the heat transferred per unit area per unit time, becomes

$$f(t) = \frac{1}{2\pi \, a \, \Delta z} \frac{d}{dt} Q(t) \tag{5.14}$$

$$= \frac{c\rho}{2\pi a} \frac{d}{dt} \int_a^\infty \Delta T(r,t)(2\pi \, rdr) \tag{5.15}$$

$$= \frac{c\rho}{a} \int_a^\infty \frac{\partial T(r,t)}{\partial t} \, r \, dr \tag{5.16}$$

Equation 5.16 can be discretised to give $f(t)$ as a vector at discrete time points. This was achieved using a central difference method to produce the temporal derivative

and Simpson's method (Garcia, 2009) to evaluate the spatial integral. Logarithmically spaced grids for both r and t were used to give increased resolution for small values. Carslaw and Jaeger (1959) graph the non-dimensionalised solution for the flux through the cylinder. Their graph is presented along side the flux calculated numerically in this study in Figure 5.8, allowing a second check of coding accuracy

(a) (b)
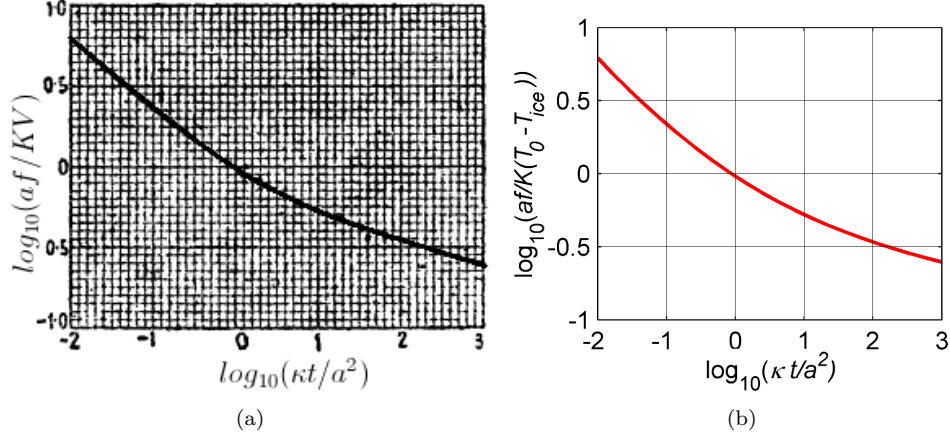
Figure 5.8: (a) Flux through a cylindrical surface $r = a$ kept at a constant temperature V with zero initial temperature outside. (b) Flux through the same surface for a constant surface temperature T_0 and initial temperature T_{ice} outside. Both vertical axes are equivalent with (a) being a special case of (b). Note: for the bore hole one day is equivalent to $\kappa t/a^2 \approx 1$.

5.6 Initial Conditions

Until now the initial horizontal temperature distribution was taken to be T_{ice}. This does not account for the thermal energy added to the surrounding ice during drilling. If this were ignored the flux calculated in the previous section would be too large. Drilling of the pilot hole will add some thermal energy to the surrounding ice but the smaller diameter means most of the heat added will go into ice that is later reamed. From here on drilling of the pilot hole will be ignored.

At each depth the initial condition will be dependent on the difference in time (Δt) between the reamer first reaching a certain depth (t_{ream}) and the nominated time at which closure starts (t_0). This is taken as the time at which the drill was removed from the hole. The reaming for the first and second use of the hole took 380 minutes and 230 minutes respectively. The reamer is descending for approximately 60% of each of those times. By the time reaming was completed for the second use of the hole it had been kept open for 114 hours. This will be the value taken for t_0. Therefore the model will predict slower growth the second time the hole closes.

5.7 Closure Rate

The heat flux into the ice as a function of time is now known (Equation 5.16) along with the flux of latent heat for a volume, V, of ice growth (Equation 5.7). These two can be equated to find the closure rate.

$$f_{latent} = f_i = \phi \rho L_f \frac{dV}{dt} \frac{1}{2\pi a \Delta z}$$

(5.17)

37

An application of related rates of change finds dV/dt in terms of the desired quantity, dR/dt.

$$\frac{dV}{dt} = \frac{dV}{dR}\frac{dR}{dt} = 2\pi\,R\,\Delta z\frac{dR}{dt} \tag{5.18}$$

This leads to

$$\phi\rho L_f\frac{R}{a}\frac{dR}{dt} = f_i(t) \tag{5.19}$$

$$\int_a^R R'dR' = \frac{a}{\phi\rho L_f}\int_0^t f(t')dt' \tag{5.20}$$

$$R(t) = \sqrt{a^2 - \frac{2a}{\phi\rho L_f}\int_0^t f(t')dt'} \tag{5.21}$$

5.8 Solid Fraction

The only model parameter left to be found is the solid fraction of ice. As described in Section 3.3 the details are not well known. Freezing will occur at all points in the annulus of refrozen ice, but the model will treat the average of this growth and assume all growth occurs at the interface. There appears to be no study of refrozen ice structure in bore holes in the literature that could be applied here. Instead two arguments are given to show that the most practical estimate of the solid fraction is ϕ = 0.4.

5.8.1 Solid Fraction of Platelet Ice

The structure of platelet ice under sea ice is similar to what might be expected for the ice forming on the sides of bore holes. Using platelet ice as an analogue to ice that forms in a bore hole is advantageous as a number of studies have been undertaken to find the solid fraction of this layer. The platelet layer forms with a similar mechanism but direct application of the results into the context of bore holes must be treated with care because platelet ice forms against a horizontal plane whereas the side of a bore hole is vertical. Both ice structures grow under two main processes.

1. Ice forms as heat transfers through the ice/water interface.

2. Ice forms when ice crystals suspended in water attach to the interface.

Gough et al. (under review) determine the solid fraction in the platelet layer using measurements of heat flux from sea ice temperature profiles. They calculate a value of $\phi = 0.25 \pm 0.06$, as well as collating values found from six other papers that use a variety of methods. It is expected that ice in the bore hole would have a higher solid fraction because not all of the ice suspended in the water column will become attached at the interface. Therefore $\phi = 0.25$ could be taken as the lowest possible value.

5.8.2 Measured Closure Rates

Makinson (1993) graphs the closure rate for a bore hole in the Ronne Ice Shelf two days after drilling. Unfortunately, details of the drilling process and the hole's initial radius are not clearly stated which means an accurate assessment from the measurements can not be found. With regard to a different field study he states that initial closure rates of 9 to 11 mm diameter hr^{-1} were recorded for a 0.13 m diameter bore hole in ice at $-26°$C. These measurements were taken "shortly after the hole had been drilled". If the time of measurement had been stated more accurately then the solid fraction could have been derived by applying the model of the present study to this smaller bore hole.

Instead the model was applied to several times that may have represented "shortly after drilling". Without accurate times my investigation was only able to constrain the range of the solid fraction to $0.3 < \phi < 0.6$ with the most likely value being $0.35 - 0.45$. From here on the value 0.4 will be taken as the solid fraction. It is worth noting that if the flux in Equation 5.21 were taken to be constant then the total closure time would be directly proportional to ϕ.

5.9 Results

The result of applying the calculations discussed in this chapter are shown in Figure 5.9 for both the first and second use of the hole. An interesting aspect of the result is that the first part of the hole to reach complete closure is not the top of the hole as might be expected from considering only temperature profiles. Rather the bubbly ice near the surface reduces the rate of heat transfer such that the hole first closes at a distance of $30 - 40$ metres below the water surface.

(a)

(b)
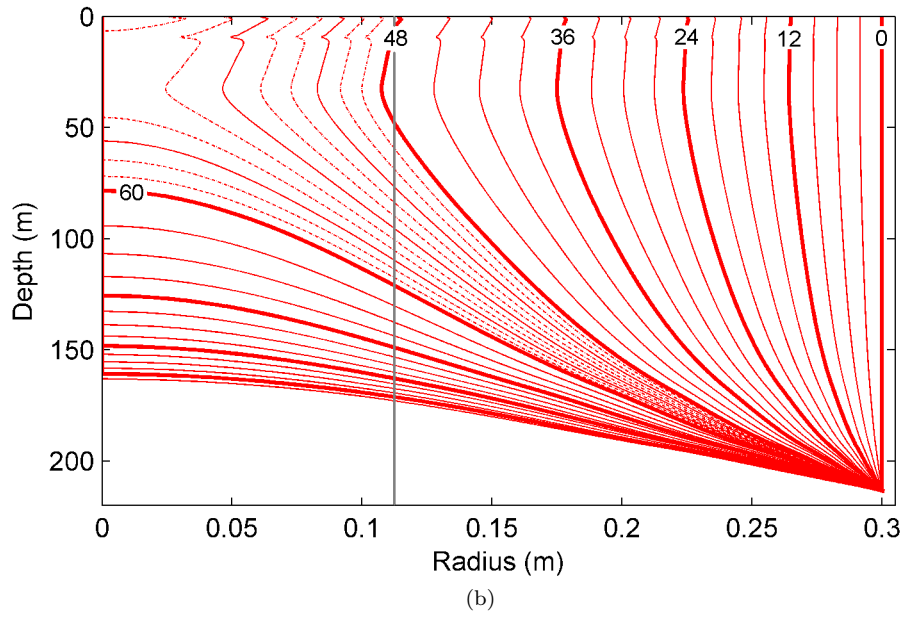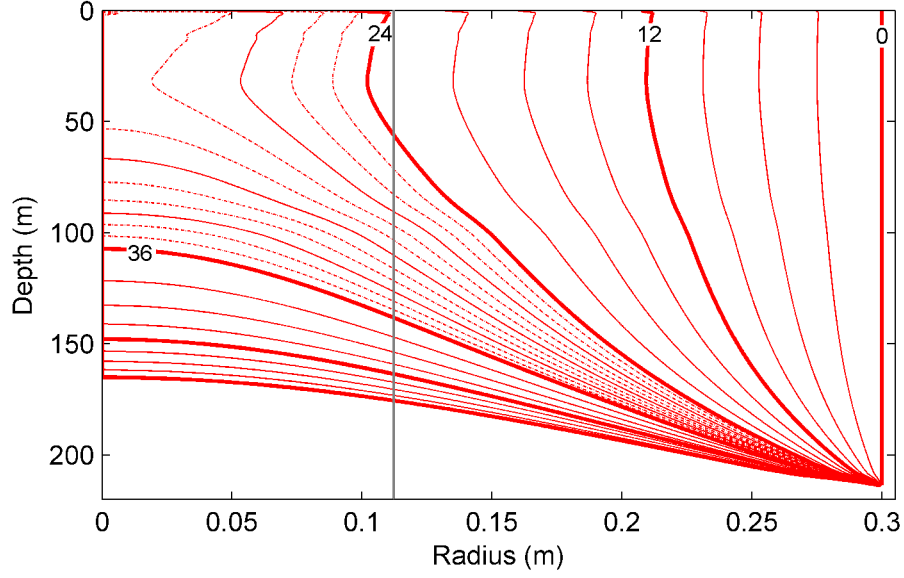
Figure 5.9: Evolution of the bore hole radius (R) after reaming on (a) 8th December and (b) 12th December. Thin lines are separated by 3 hours and thick lines by 12 hours. Higher resolution is shown near closure by the dotted lines (separated by hours). The vertical grey lines represents the critical radius determined by the maximum width of the CTD profiler (see Section 1.2). ($\phi = 0.4$)

Chapter 6

Discussion

6.1 Comparison of Models

We are now in a position to compare the two models of refreezing formulated in the previous chapters. It will be shown that each model has its own merits but the best prediction of refreezing would come about through a combination of the results.

The models are formulated upon different assumptions. The salinity variation model (SVM) is based on measurements of the water properties. It assumes that all dissolved salt is rejected from the ice formed and the water column is a closed system, absent of large scale mixing processes and homogeneous in any horizontal plane. The heat flux model (HFM) assumes only conduction in the host ice, only convection in the refrozen ice, no vertical heat fluxes and a constant water temperature.

A graphical comparison of the models is shown in Figure 6.1; the rates predicted by each are shown for both dates. There are three important things to note about this figure.

- The rate derived from the HFM is averaged over the first 24 hours of closure for each of the dates whereas that from the SVM is averaged over the time in which this model was run (approximately $18 - 42$ hours). It is not possible to run the models over the same period as the HFM predicts closure occurs before 42 hours on December $8 - 9$.

- The radius of the hole at the time the SVM model begun affects the closure rates it predicts. It was taken to be 0.25 m at every depth as opposed to 0.3 m for the HFM. The decrease of 5 cm represents an approximation of the growth that would have occurred before the SVM started.

- Inspection of Figure 4.2a shows that the SVM gives an unphysical prediction of a large amount of melting throughout the bore hole over the last time step on $8 - 9$ December but this is due to an unexpected result in only the last salinity cast. It significantly affects a prediction of the average closure rate which would unfairly skew comparisons between the models. For this reason it will not be used in the refreezing rate calculation.

Magnitude of Predicted Rates

The two models predict refreezing rates of the same magnitude and the results are especially close for the rates predicted on 13 –14 December.

It is known that the heat flux model overestimated the ice growth the first time the hole refroze. No direct measurements of the refreezing rates were made on site
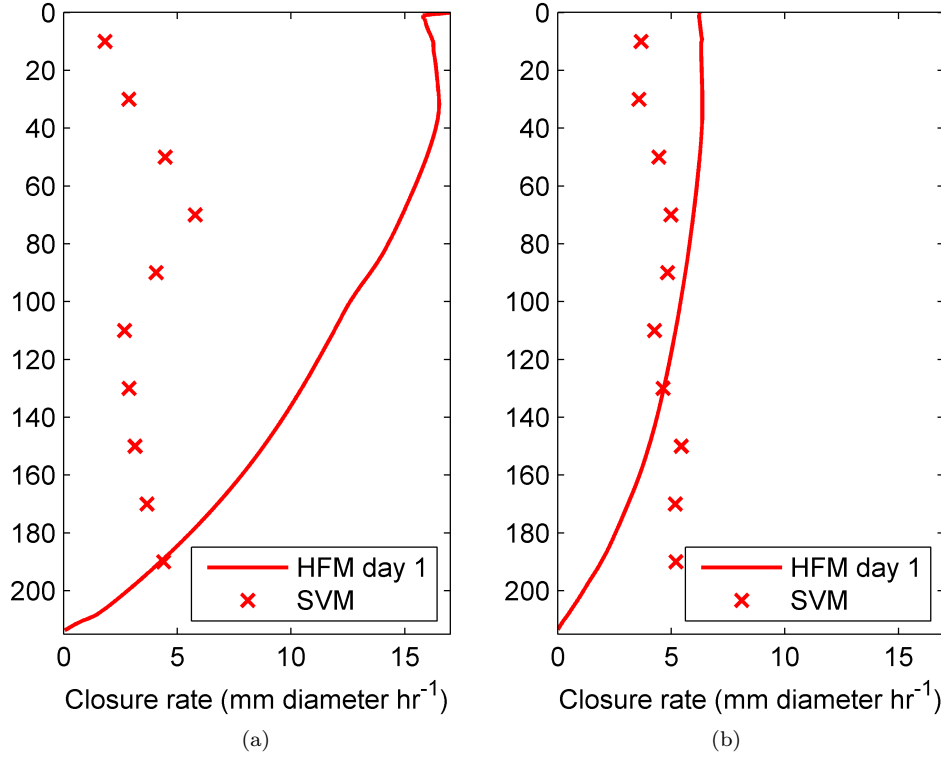
Figure 6.1: Rates of closure predicted by this study for (a) $8 - 9$ December and (b) $13 - 14$ December. The closure rate predicted by the salinity variation model (SVM) is averaged over both the time the model was run and 20 m increments in depth. The closure rates of the heat flux model (HFM) are averaged over the first 24 hours after reaming. ($\phi = 0.4$)

but the hole would have been larger than the critical diameter at the time the CTD measurements ended. This critical diameter, dictated by the maximum width of the CTD profiler, is 225 mm. Figure 5.9a shows that the hole is predicted to fall below this value after 24 hours, whereas CTD measurements finished after $44 - 45$ hours. Figure 5.9b shows that a drop below this critical diameter almost occured on $13 - 14$ December as well.

The SVM predicts rates lower than the HFM on $8 - 9$ December. For this reason the SVM appears to give better results because it would not predict that the hole diameter falls below critical before retrieval of the CTD profiler. On $13 - 14$ December both models predict very similar rates. In fact, if the result of each model were averaged from the surface to a depth of 200 m the rates would agree to within 5%. Some of this can be attributed to sheer luck, especially since the models are not applied over exactly the same time periods. However, it gives confidence in the models because they were formulated in very different ways yet produce similar results.

6.2 Features of the Results

There are a number of features, some unwanted, of the results that are independent of the actual refreezing rate predicted.

First Depth to Refreeze

The HFM predicts that at any particular time the maximum rate of closure occurs at a depth of $30 - 40$ m. This is a consequence of the way ice shelf parameters vary with depth, but must be treated with some caution. The variation of some parameters was from measured data (from 1958) while the variation of other parameters was modelled.

Different Initial Conditions

The length of time that the bore hole has previously been kept open is an important factor in predicting closure rates. As time goes on the temperature of the surrounding ice increases, tending toward the temperature of water in the bore hole. The flux of heat into the ice is very high at the moment the hole is drilled. It decreases rapidly thereafter but approaches a nearly constant value after a few days. When the hole refroze a second time after being kept open for approximately five days it took almost twice as long to reach complete closure.

Periods of Melting

The SVM model predicts some periods of hours or more in which melting and/or no refreezing occurs during $8 - 9$ December. This is an unphysical result but can be attributed to the fact that the model is using experimental data. There may have been factors not considered in this study leading to these anomalous results. Also, it has previously been stated that the SVM is more likely to accurately model refreezing during $13 - 14$ December when the water column is more stable. As desired it predicts the radius will decrease monontonically during this time (ignoring one small fluctuation).

It is important to note that this model was never expected to produce accurate results for the top and bottom of the bore hole. For depths of 20 m or less the geometry of the bore hole is affected by the well. In this region it is invalid to model the bore hole as a cylinder. However, the dimensions of the bore hole were unknown so could not be treated. Furthermore, applying the model to a geometry that lacks symmetry would be more complex. For depths close to the base of the ice shelf there is a large salinity gradient tending toward seawater salinity. This could imply a significant interaction with the ocean below that was ignored by treating the hole as a closed system.

Depth Dependence of Predicted Rates

The refreezing rate should be expected to show some dependence with depth. More specifically, it would be expected to freeze most quickly near the top where the ice shelf is the coldest. This is very apparent in the HFM, as shown in Figure 6.1. However, the SVM shows no obvious variation with depth; it is not possible to say more than that it is predicts approximately constant growth throughout the bore hole.

Figure 6.2 shows that direct caliper measurements of closure rates of a bore hole in the Ronne Ice Shelf confirm that this result, expected from the HFM, does occur. Repeated reaming of the hole may significantly affect the vertical temperature distribution of the ice surrounding the bore hole. Thus, Figure 6.2 does not necessarily confirm the expected depth dependence for refreezing on $13 - 14$ December.

6.3   Role of the Solid Fraction

A particularly important unknown in both models is the solid fraction ϕ; at any time refreezing rates are directly proportional to its value. The time of complete closure is almost directly proportional to its value also, but there is some non-linearity due to the decrease in flux over time. An underestimation of its value leads to an overestimation
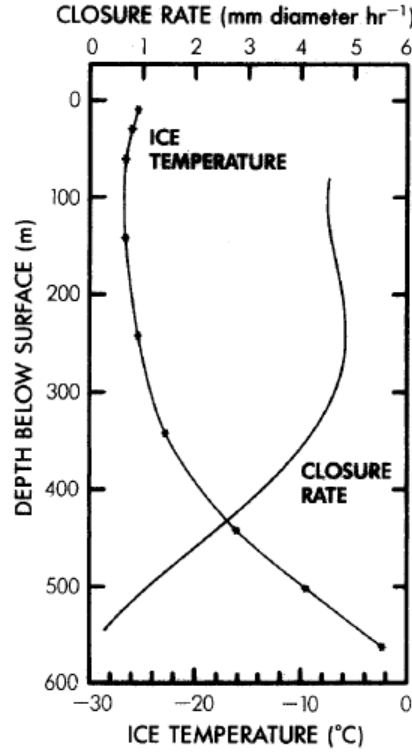
Figure 6.2: Ice temperature and closure rates of a 540 m deep bore hole drilled two days earlier in the Ronne Ice Shelf. The diameter ranged between 0.14 m and 0.2 m. (Duplication of Figure 5 from Makinson (1993))

of the time of closure and vice versa. The effect of the variation in ϕ can be seen in Figure 6.3 where, as an example, the HFM was applied for five possible values to predict closure at a depth of 100 m immediately after reaming. This figure exemplifies how such a small change in the value of ϕ can propagate into a large range of possible complete closure times. The value chosen affects the SVM in the equivalent way.

Figure 6.3 indicates that the previously described problem of overestimates of closure rates from the HFM could have arisen due to an overestimate of ϕ. However, this is only speculation.

6.4 Coding Efficiency

The cylindrical symmetry and large aspect ratio of the bore hole was exploited in both models, allowing each to be computationally efficient. The heat flux model required a significantly larger amount of coding but it would still be possible to formulate this model in a single MatLab script that could produce all of the results shown in Chapter 5 but requiring only a few minutes of computation. This speed can be largely attributed to the efficiency of the `pdepe` routine (MathWorks Inc., 2008) used.

6.5 Application to Different Bore Holes

A major focus of this study is to simulate the refreezing of the NIWA bore hole but it is desirable to apply the models elsewhere. The SVM does not generalise easily to other bore holes because it is inherently reliant on experimental data as input. The
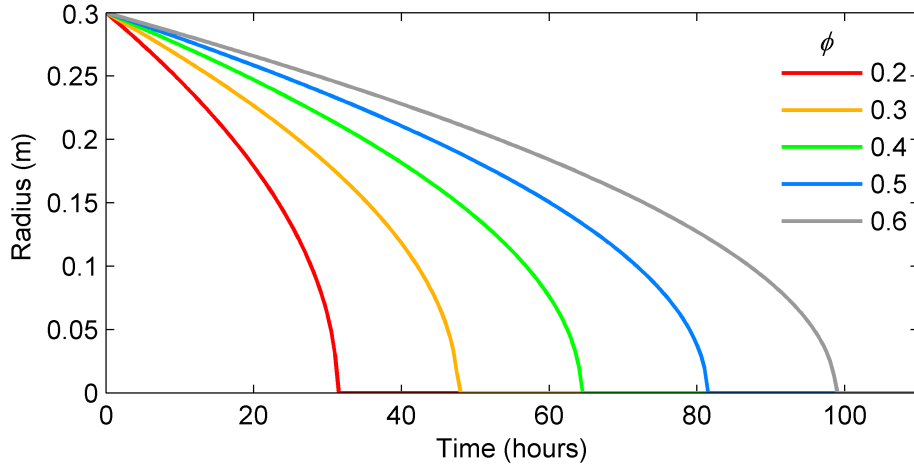
Figure 6.3: Example of the affect of the value of ϕ in the models of this study. This figure shows closure of the bore hole immediately after reaming for values of ϕ between 0.2 and 0.6. The value of 0.4 was used for all results produced in this study.

calculation of the refreezing rate acts only to predict an expected rate for a similarly sized bore hole in a similar location. Conversely, application of the HFM to an alternative site is possible, albeit not straightforward. It requires knowledge of the values, and their variation with depth, of all parameters listed in Table 5.1.

The simplest way to apply the HFM at a different location would be to find temperature and density profiles, at or near the alternative site, from the literature and then proceed with the methods specified in Chapter 5. However, there are very few of these profiles available for Antarctic ice shelves (personal communication, A. Humbert).

The alternate solution is to assume all Antarctic ice shelves have the same structure. Then it is possible to adopt the profiles given in Chapter 5 which can be vertically scaled to fit the thickness of the ice shelf in question. Consider the vertical temperature profile as an example of the validity of this method. Humbert et al. (2005) used a vertical scaling of a single parabolic fit to model the temperature profile for the entire Ross Ice Shelf. Furthermore, Makinson (1993) presents the temperature profile through the Ronne Ice Shelf (Figure 6.2) which, despite being almost twice as thick and having a different surface temperature, has a very similarly shaped profile. If it is assumed that the profiles of all parameters show this scaling behaviour then it would be possible to implement this model elsewhere by knowing only the temperature in the top section of the ice shelf, for which there are a number of data sets e.g. MacAyeal et al. (2008).

Some parameters may even be treated as constant. For example T_0 can not be known without a CTD profile being taken but because its range is only a few degrees it could be taken as say -1°C everywhere without the loss of much accuracy.

Overall, the two models predict rates of similar magnitude but only the HFM could be used in advance to predict refreezing of a bore hole of different dimensions and/or at a different location.

Chapter 7

Summary and Conclusion

7.1 Summary

Two models were created to calculate the rate of refreezing of a bore hole drilled in the Ross Ice Shelf. The first model, based on the use of CTD recordings involved some generalisations and ignored potentially interesting properties of the water inside the bore hole yet still managed to predict likely refreezing rates. The second model, based on heat conduction theory, predicted what appeared to be overestimates of the refreezing rate at any depth and time. It differed from similar models found in the literature by including the variation with depth of a number of variables involved in the heat equation.

Two different initial conditions were considered in this study; closure was modelled both immediately after reaming of the hole and after the hole had been kept open for approximately five days. The models predicted similar refreezing rates for the latter. Conversely, for closure immediately after reaming the salinity model appeared to give the better estimate.

The amount of time a bore hole takes to refreeze is dependent on the structure of the refrozen ice. In this study the treatment of this structure was reduced to the estimate of a single parameter, ϕ, by assuming that ice freezes with a porous structure and that a fixed fraction of solid ice grows in any volume of water. Closure rates have a linear dependence on ϕ so the results returned by the model are sensitive to the value chosen.

With a more sophisticated treatment of the structure of the refrozen ice this model could be expected to accurately predict closure rates of bore holes of any height and diameter in any Antarctic ice shelf.

7.2 Future Work

The treatment of the refrozen ice is the largest factor that requires further attention; its formation mechanism and structure were analysed only simply in this study. A more in depth investigation of these will allow more accurate modelling of the closure and help quantify the error associated with the results of this model. Particular improvements or possible experiments that could be investigated are listed below.

- It may be that the structure is dependent on the extent to which freezing has already occurred. Therefore, a value of ϕ that changes with radius and/or time could be incorporated.

- It may be possible to imitate bore hole conditions in the lab, although there would be a significant challenge in simulating the large depths involved. This

would allow estimates of the solid fraction and thermal properties of the refrozen ice.

- Direct measurements of the closure rates could be taken to compare with the theoretical rates. This could be achieved with caliper measurements as described in Makinson (1993) or with estimates from video recordings.

- Treating the ice as a porous structure and modelling heat transfer through it is possible, albeit mathematically complex.

There are three properties of the water in the bore hole which were not investigated in this study. No attempt will be made to explain these properties in detail but they could prove interesting with further study.

- The salinity profiles taken on 8 – 9 December (Figure 3.6) show a large salinity gradient at a depth of 80 – 100 m. Possibly an artefact of drilling.

- Also in the first set of salinity profiles the salinity decreases between depths of 100 m and 200 m. This would lead to a decrease in density with an increase in depth. It would be expected that this feature would cause instability, but instead this feature persists over time measurements were being taken. The dependence of this on the geometry of the hole could be investigated.

- A cusp is shown on the salinity profiles taken on the 13/14th December. This feature persists over the time of the 10 casts.

7.3   Conclusion

The value of the SVM is that it provides closure rates, derived from data, that broadly confirm the predictions of the HFM in the case of refreezing of the NIWA bore hole in the Ross Ice Shelf. We can have confidence in their validity as they gave similar predictions, especially when predicting closure on 13 – 14 December. This is a remarkable result given the models were formulated in completely different ways.

Bibliography

G. K. Batchelor and J. M. Nitsche. Instability of a Stratified Fluid in a Vertical Cylinder. *J. Fluid Mech.*, 252:419–448, 1993.

J. A. Bender and A. J. Gow. Deep Drilling in Antartica. *Int. Assoc. Hydrol. Sci.*, 55: 132–141, 1961.

H. S. Carslaw and J. C. Jaeger. *Conduction of Heat in Solids. Second Edition.* Clarendon Press, Oxford, 1959.

A. Colling. *Ocean Circulation. Second Edition.* Butterworth Heinemann, Boston, 2001.

D. E. Dempsey, P. J. Langhorne, N. J. Robinson, M. J. M. Williams, T. G. Haskell, and R. D. Frew. Observation and Modeling of Platelet Ice Fabric in McMurdo Sound, Antarctica. *J. Geophys. Res.*, 115:doi:10.1029/2008JC005264, 2010.

D. J. Drewry. *Antarctic Geological and Geophysical Folio.* Scott Polar Research Institute, 1983.

H. Engelhardt, B. Kamb, and R. Bosley. Instruments and Methods. A Hot -water Ice-coring Drill. *J. Glac.*, 46(153):341–345, 2000.

P. Fofonoff and R. Millard. Algorithms for Computation of Fundamental Properties of Seawater. *Unesco Tech. Pap. in Mar. Sci.*, 44(53), 1983.

D. Garcia. MatLab: cumsimps, 2009. URL http://www.mathworks.com/matlabcentral/fileexchange/ 25754-simpsons-numerical-integration.

H. Goldenberg. Some Numerical Evaluations of Heat Flow in the Region Bounded Internally by a Circular Cylinder. *Proc. Phys. Soc.*, 69:256–260, 1956.

A. J. Gough, A. Mahoney, P. J. Langhorne, M. J. Williams, N. J. Robinson, and T. G. Haskell. Signatures of Supercooling: McMurdo Sound Platelet Ice. *J. Glac.*, 00:–, under review.

M Grasselli and D Pelinovsky. *Numerical Mathematics.* Jones and Bartlett Publishers, Sudbury, MA, 2008.

R. Greve and H. Blatter. *Dynamics of Ice Sheets and Glaciers.* Springer, 2009.

W. D. Harrison. Temperature of a Temperate Glacier. *J. Glac.*, 11(61):15–29, 1972.

W. M. Haynes. *CRC Handbook of Chemistry and Physics.* CRC Press, 91st edition, 2010.

H. Hoinkes. Studies in Glacial Meteorology at Little America V, Antartica. *Internat. Assoc. Scient. Hydrology Publ.*, 55:29–48, 1961.

D. M. Holland and A. J. Jenkins. Modeling Thermodynamic Ice-Ocean Interactions at the Base of an Ice Shelf. *J. Phys. Oceanogr.*, 29:1787–1800, 1999.

A. Humbert, R. Greve, and K. Hutter. Parameter Sensitivity Studies for the Ice Flow of the Ross Ice Shelf, Antartica. *J. Geophys. Res.*, 110:F04022, 2005.

N. Humphrey and K. Echelmeyer. Hot Water Drilling and Bore-Hole Closure in Cold Ice. *J. Glac.*, 36(124):287–298, 1990.

E. H. Huppert and E. G. Josberger. The Melting of Ice in Cold Stratified Water. *J. Phys. Oceanogr.*, 10:953–960, 1980.

IOC, SCOR, and IAPSO. *The International Thermodynamic Equation of Sea Water - 2010: Calculation and Use of Thermodynamic Properties.* Intergovernmental Oceanographic Commision, Manuals and Guides No. 56, UNESCO.

F. Kreith and F. E. Romie. A Study of the Thermal Diffusion Equation with Boundary Conditions corresponding to Solidification or Melting of Materials Initially at the Fusion Temperature. *Proc. Phys. Soc*, 68:277–291, 1955.

P. K. Kundu and I. M. Cohen. *Fluid Mechanics. Second Edition.* Academic Press., 2002.

G. H. Leonard, C. R. Purdie, P. J. Langhorne, T. G. Haskell, M. J. M. Williams, and R. D. Frew. Observations of Platelet Ice Growth and Oceanographic Conditions during the Winter of 2003 in McMurdo Sound, Antartica. *J. Geophys. Res.*, 111: doi:10.1029/2005JC002952, 2006.

D. MacAyeal, O. Sergienko, T. Scambos, and A. Muto. Ross Ice Shelf firn temperature, Antarctica. Digital Media, 2008.

K. Makinson. The BAS Hot Water Drill: Development and Current Design. *Cold Reg. Sci. Technol.*, 22(1):121–132, 1993.

The MathWorks Inc. *MatLab Version 7.6.0.* Natick, Massachusetts, 2008.

P. Morgan. The SeaWater Matlab library., 2003. URL `http://www.cmar.csiro.au/datacentre`.

J. G. P. Napoleoni and G. K. C. Clarke. Hot Water Drilling in a Cold Glacier. *Can. J. Earth Sci*, 15(2):316–321, 1978.

W. S. B Paterson. *The Physics of Glaciers.* Pergamon Press, 1969.

C. Petrich, P. J. Langhorne, and T. G. Haskell. Formation and Structure of Refrozen Cracks in Land-fast First-year Sea Ice. *J. Ge*, 112:C04006, doi:10.1029/2006JC003466., 2007.

G. Poots. On the Application of Integral Methods to the Solution Problems Involving the Solidification of Liquids Initially at Fusion Temperature. *Int. J. Heat Mass Transfer.*, 5:525–531, 1962.

J.P. Rafferty. *Glaciers, Sea Ice and Ice Formation.* Brittanica Educational Publishing, 2011.

P. Schwerdtfeger. The Thermal Properties of Sea Ice. *J. Glac.*, 4(36):789–807, 1963.

L. H. Smedsrud and A. Jenkins. Frazil Ice Formation in an Ice Shelf Water Plume. *J. Geophys. Res.*, 109:doi:10.1029/2003JC001851, 2004.

S. Tsutaki and S. Sugiyama. Developments of a Hot Water Drilling System for Subglacial and Englacial Measurements. *Bull. Glaciol. Res.*, 27:7–14, 2009.

UNESCO. The Practical Salinity Scale 1978 and the International Equation of State of Seawater 1980. Tenth Report of the Joint Panel on Oceanographic Tables and Standards. *Unesco Tech. Pap. In Mar. Sci*, UNESCO, Sidney, B.C., 1980.

W. F. Weeks. *On Sea Ice*. University of Alaska Press, 2010.

Appendix A

The Salinity Scale and Equations of State

This study uses the Practical Salinity Scale 1978, PSS-78, and the International Equation of State of Seawater 1980, EOS-80 (UNESCO, 1980) and a number of algorithms derived from these (Fofonoff and Millard, 1983). The definitions and equations relevant to this study are summarised below.

Table A.1: Values of the constants for the algorithms below.

$a_0 = -0.0080$	$b_0 = 0.0005$	$c_0 = 0.6766097$
$a_1 = -0.1692$	$b_1 = -0.0056$	$c_1 = 2.00564 \times 10^{-2}$
$a_2 = 25.3851$	$b_2 = -0.0066$	$c_2 = 1.104259 \times 10^{-4}$
$a_3 = 14.0941$	$b_3 = -0.0375$	$c_3 = 6.9698 \times 10^{-7}$
$a_4 = -7.0261$	$b_4 = 0.0636$	$c_4 = 1.0031 \times 10^{-9}$
$a_5 = 2.7081$	$b_5 = -0.0144$	

$d_0 = 4.8314 \times 10^{-4}$		
$d_1 = 3.426 \times 10^{-2}$	$e_1 = 2.070 \times 10^{-4}$	$f_1 = -0.0575$
$d_2 = 4.464 \times 10^{-4}$	$e_2 = -6.370 \times 10^{-8}$	$f_2 = 1.710523 \times 10^{-3}$
$d_3 = 4.215 \times 10^{-1}$	$e_3 = 3.989 \times 10^{-12}$	$f_3 = -2.154996 \times 10^{-4}$
$d_4 = -3.107 \times 10^{-3}$		$f_4 = -7.53 \times 10^{-4}$

The following equations require temperature in °C, pressure (above atmospheric pressure) in bars and salinity in Practical Salinity Units (PSU).

A.1   Salinity

The salinity, S, of seawater is defined in terms of the ratio of the conductivity of a sample at 15°C and one standard atmosphere, to that of a potassium chloride solution with a mass fraction of 32.4356×10^{-3}. In situ measurements produce the quantity R, the ratio of the in situ conductivity to the standard conductivity at $S = 35$, $T = 15$°C and $P = 0$ bar.

$$R_t = \frac{R}{R_p r_t} \tag{A.1}$$

where R_t is the ratio of the conductivity of seawater, at temperature T, to the conductivity of seawater with $S = 35$ PSU at the same temperature and

$$R_p = 1 + \frac{P(e_1 + e_2 P + e_3 P^2)}{1 + d_1 T + d_2 T^2 + (d_3 + d_4 T)R} \tag{A.2}$$

$$r_t = c_0 + c_1 T + c_2 T^2 + c_3 T^3 + c_4 T^4 \tag{A.3}$$

Salinity is found from R_t by

$$S = a_0 + a_1 R_t^{1/2} + a_2 R_t + a_3 R_t^{3/2} + a_4 R_t^2 + a_5 R_t^{5/2} + \Delta S \tag{A.4}$$

$$\Delta S = \frac{T - 15}{1 + 0.0162(T - 15)} \left(b_0 + b_1 R_t^{1/2} + b_2 R_t + b_3 R_t^{3/2} + b_4 R_t^2 + b_5 R_t^{5/2} \right) \tag{A.5}$$

A.2 Density

The density of seawater is given by the equation of state. At one standard atmosphere $(P = 0)$, as a function of temperature and salinity, it is given by

$$\rho(S, T, P = 0) = \rho_w + (b_0 + b_1 T + b_2 T^2 + b_3 T^3 + b_4 T^4)S \tag{A.6}$$
$$+ (c_0 + c_1 T + c_2 T^2)S^{3/2} + d_0 S^2$$

where ρ_w is the density of pure water at temperature T.

The density at any pressure is then

$$\rho(S, T, P) = \frac{\rho(S, T, 0)}{1 - \dfrac{P}{K(S, T, P)}} \tag{A.7}$$

where $K(S, T, P)$ is the secant bulk modulus (a measure of resistance to compressibility of a fluid). More detail for this complex algoritm can be found in Fofonoff and Millard (1983).

A.3 Freezing Point

The freezing point as a function of salinity and pressure is

$$T_f = f_1 S + f_2 S^{3/2} + f_3 S^2 + f_4 P \tag{A.8}$$

Appendix B

Treatment of Raw Data

The raw data used for this study was two sets of 10 CTD casts. During each cast the CTD profiler descended from the water surface to the bottom of the hole once and from the base of the ice shelf to the ocean floor three times. Measurements were taken, at a frequency of 4 Hz, as the CTD profiler moved both upward and downward. Only the profile recorded during descent was used in this study, giving profiles approximately evenly spaced in time.

Pressure Offset

The CTD profiler did not measure exactly 0 dbar at the beginning of each cast. Rather, there was an offest in each cast of the order of 1 dbar. This was removed by taking the average of the first 20 measurements in air and subtracting this offset from the subsequent pressure measurements.

Ice Shelf Base

The base of the ice shelf was determined from an abrupt change in potential density, found to be at 211.5 dbar which corresponds to a depth of 213 m. Therefore, the profiles were truncated after this point ensuring only measurements in the hole were used.

Depth from Pressure

The salinity changed significantly in the hole and thus the usual technique to convert pressure to depth could not be used. Instead, depth (z_i) was related to a cumulative sum of density values which were found from the equation of state (UNESCO, 1980). The use of a more accurate numerical integration technique was not needed as the high frequency of measurements gave high spatial resolution. Depth was found from the following equation.

$$z_i = \sum_{n=1}^{i} \frac{P_n}{g\,\rho(S_n, T_n, P_n)} \tag{B.1}$$

Data Binning

The data of each cast were binned into 0.2 m increments with a moving average to produce easy to manage data sets. The values of salinity, temperature, pressure and density were found at every depth by taking the mean of all recordings within 1 m of that depth.

Appendix C

Instrumentation

The data used in this study was recorded by a Seabird Electronics SBE 19*plus* SEACAT Profiler fitted with an SBE 38 dissolved oxygen (DO) sensor. A brief description of the CTD profiler will be given here, more detail can be found on the manufacturer's website (www.seabird.com).

Figure C.1: Seabird SBE-19*plus* CTD profiler. Photo taken from the User's Manual.

Table C.1: SBE-19*plus* specifications from the manufacturer. Conductivity resolution equates to 0.004 ppm in salinity. f.s.r. refers to the full scale range; this model was rated to 1000 m. It can be taken as any of 20/100/350/600/1000 m.

	Temperature ($^\circ$C)	Conductivity (S/m)	Pressure
Range	-5 to 35	0 to 9	upto 7000 m
Initial Accuracy	0.005	0.0005	0.1% of f.s.r.
Resolution	0.0001	0.00005	0.002% of f.s.r.

The maximum width, height and length of the profiler (without the attached DO sensor) are 103 mm, 136 mm and 808 mm respectively. During the experiment it was mounted in a circular frame of diameter 225 mm and length 1048 mm.

Appendix D

Salinity Model Iteration

$$R_{i+1} = R_i \sqrt{\frac{\rho_i S_i - \rho_{i+1} S_{i+1}(1 - \phi)}{\rho_i S_i \phi}}$$

Inspection of Equation 4.6, restated above, shows that the radius at any value of t_{i+1} is dependent on the current radius and the present and next set of values of salinity and density. The simplest way to determine the radius at any time would be to loop through the equation using the data of each CTD cast to find the radius at each value of t_i and use linear interpolation for all other values of time. However this means that any unexpected salinity or density measurement will skew all subsequent values of the radius. When the data was treated this way it lead to the unphysical result that the interface sometimes showed periods of melting.

Calculating a result from Equation 4.6 has a very close analogue to the process of numerically solving a first order differential equation. The above description is most similar to the Euler method, which is known to have a large truncation error. However, unlike a differential equation a value for the gradient (here the rate of ice growth) at points in between the time steps cannot be determined. Therefore a predictor-corrector scheme, adapted from the Heun method is used. The Heun method requires that the function need only be known at the time points themselves. In the context of numerical differential equations this method has a truncation error of second order (Grasselli and Pelinovsky, 2008). The use of a higher order method such as the fourth order Runge Kutta method is precluded as input variables are not known in between time points.

In its simplest form Equation 4.6 says $R_{i+1} = f(S_i, \rho_i, S_{i+1}, \rho_{i+1})R_i$, where f is the square-root term. The procedure finds R_{i+1} by first calculating the intermediate values $\widetilde{R}_{i+1}$ and $\widetilde{R}_{i+2}$ directly from Equation 4.6. R_{i+1} is then the average of these, weighted by their respective time differences, $t_{i+1} - t_i$ and $t_{i+2} - t_{i+1}$.

Mathematically this is stated as

$$\widetilde{R}_{i+1} = f(S_i, \rho_i, S_{i+1}, \rho_{i+1})R_i \tag{D.1}$$

$$\widetilde{R}_{i+2} = f(S_{i+1}, \rho_{i+1}, S_{i+2}, \rho_{i+2})\widetilde{R}_{i+1} \tag{D.2}$$

Letting $\Delta t_i = t_{i+1} - t_i$

$$R_{i+1} = \frac{1}{2}\left(\frac{\widetilde{R}_{i+1}}{\Delta t_i} + \frac{\widetilde{R}_{i+2}}{\Delta t_{i+1}}\right)\Delta t_i \tag{D.3}$$

The final value for the radius is found from Equation 4.6 using the Euler type method as there is no set of values of S_{i+2} and ρ_{i+2}.

Appendix E

Implementation of Heat Flux Calculation

The model described in chapter four was based around the use of the built-in MatLab routine `pdepe` (MathWorks Inc., 2008). This can solve parabolic-elliptic partial differential equations with slab, cylindrical or spherical symmetry. `pdepe` was used to find the temperature distribution from which the heat flux can be derived.

E.1   Use of pdepe

The Partial Differential Equation

`pdepe` requires the problem be formulated in a specific way. The general differential equation it solves is

$$c\left(x, t, u, \frac{\partial u}{\partial x}\right) \frac{\partial u}{\partial t} = x^{-m} \frac{\partial}{\partial x}\left(x^m f\left(x, t, u, \frac{\partial u}{\partial x}\right)\right) + s\left(x, t, u, \frac{\partial u}{\partial x}\right) \qquad \text{(E.1)}$$

This will reproduce Equation 5.4 provided

- u and x are substituted for temperature (T) and radial position (r)

- m, the parameter describing the symmetry of the problem, is set to 1 (cylindrical symmetry).

- the last term of the equation is set to zero (it represents any heat sources).

- c becomes $1/\kappa$.

- f becomes $\partial T/\partial r$

The Initial Condition

The initial conditions must be given in the form

$$u(x, t_0) = u_0(x) \qquad \text{(E.2)}$$

where $u_0(x)$ is either a constant or a function of x. The simple initial condition described in Section 5.6 is reproduced by setting $u_0(x)$ to T_{ice}.

The Boundary Conditions

The conditions at the left and right boundary ($r = a$ and $r = \infty$) must be given in the form

$$p(x, t, u) + q(x, t)f\left(x, t, u, \frac{\partial u}{\partial x}\right) = 0 \tag{E.3}$$

The p term represents an applied boundary temperature (possibly time dependent) and the q term represents a flux through the surface.

The boundary conditions described in Section 5.4.1 are reproduced by setting

$$p_l = T_l - T_0 \tag{E.4}$$
$$q_l = 0 \tag{E.5}$$
$$p_r = T_r - T_{ice} \tag{E.6}$$
$$q_r = 0 \tag{E.7}$$

where the subscripts l and r denote the left and right boundaries respectively.

Time and Position Grids

`pdepe` requires vectors $[x_0, x_1, \ldots, x_n]$ and $[t_0, t_1, \ldots, t_f]$ specifying the points at which a numerical solution is requested. Both vectors were logarithmically spaced to provide good resolution for small values of r and t. 300 points were used for each grid and the last five values of the position grid were made very large to approximate infinity.

Non-dimensionalisation

Because the heat equation is linear it can be non-dimensionalised. This requires position and time become $r^* = r/a$ and $t^* = \kappa t/a^2$ respectively. The PDE need only be solved once and then the solution can be shifted and scaled appropriately. The problem was solved with normalised boundary conditions $T_0 = 1$ and $T_{ice} = 0$. A typical value for κ_{ice} was used and after the solution was found the time was non-dimensionalised by multiplying by κ/a^2.

Efficiency

The above formulation reduces to less than 30 lines of code and takes MatLab approximately 10 seconds to evaluate.

E.2 Flux Calculation

The result of the previous section was a 300×300 array of temperature values for non-dimensionalised, logarithmically spaced values of time and postion. The flux was calculated following the process outlined in Equations $5.14 - 5.16$. The temporal derivative in Equation 5.16 is found using a central difference.

$$\frac{\partial T(r, t)}{\partial t} \approx \left(\frac{T(r, t_{i+1}) - T(r, t_{i-1})}{t_{i+1} - t_{i-1}}\right) \tag{E.8}$$

The spatial integral is carried out with Simpson's method applied to a non-linear grid (Garcia, 2009).

Manipulating the solution gives the non-dimensionalised flux $f^* = \dfrac{af}{K(T_0 - T_{ice})}$ where f is the dimensionalised flux.

To model bore hole closure the flux must be scaled for the appropriate values of K, T_0 and T_{ice} at every depth. The cost of using non-dimensionalised results is that the

grid of dimensionalised time points $(a^2 t^*/\kappa)$ becomes different at every depth. This was resolved using interpolation to find the flux at hourly intervals for every depth with the built-in MatLab routine `pdeval` (MathWorks Inc., 2008). The purpose of `pdeval` is post processing of results obtained from `pdepe`.

The flux will change significantly over hourly intervals but it is a well behaved function and this time step is small enough to accurately apply Simpson's method to evaluate the integral in Equation 5.21.